

"Investigating the Pathogenicity and Host Interactions of *Macrophomina phaseolina*: Insights into Fungal Metabolomics and Cell Wall Immunogenicity"

Submitted in partial fulfillment of the requirements of
BITS F421T Thesis

By

**Nandini Mukherjee
ID No. 2021B1TS2563P**

Under the supervision of

**Dr. Balakumaran Chandrasekar
Assistant Professor, Department of Biological Sciences
BITS Pilani, Pilani Campus**



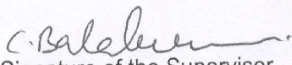
BIRLA INSTITUTE OF TECHNOLOGY AND SCIENCE PILANI, PILANI CAMPUS

10 December 2024

CERTIFICATE

CERTIFICATE

This is to certify that the thesis entitled "Investigating the Pathogenicity and Host Interactions of *Macrophomina phaseolina*: Insights into Fungal Metabolomics and Cell Wall Immunogenicity," submitted by Nandini Mukherjee bearing ID No. 2021B1TS2563P, is presented in partial fulfillment of the requirements for BITS F421T. The thesis embodies the work done by her under my supervision.



Signature of the Supervisor

Date: 10 December 2024

Dr. Balakumaran Chandrasekar
Name

Assistant Professor
Dept. of Biological Sciences, BITS Pilani
Designation

Acknowledgment

First and foremost, I would like to express my deepest gratitude to my supervisor, Dr. Balakumaran Chandrasekar, for this opportunity and his exceptional guidance, support, and encouragement throughout this research. His expertise and insights have been invaluable, and his lessons will continue to shape my professional journey.

I am also grateful to the professors and research scholars of the Department of Biological Sciences, whose courses and enthusiasm sparked my passion for this field and played a pivotal role in my academic journey.

My sincere thanks go to the members of the PTC lab for their continuous assistance and collaboration. I would like to extend a special thanks to Muthusaravanan Sir, Chetan Sir, Anirudh, and Navin, whose companionship and teamwork made this research process both enjoyable and fulfilling.

Lastly, I would like to thank everyone who has contributed, both directly and indirectly, to the completion of this thesis. Your support and encouragement have been invaluable.

Table of Contents

List of Figures.....	5
Abbreviations and Symbols.....	7
Abstract.....	8
Chapter 1: Introduction.....	9
References for Chapter 1.....	10
Chapter 2: Review of Literature.....	11
1.1 Introduction.....	11
1.2 Host Range and Economic Importance.....	11
1.3 Morphological Characteristics.....	11
1.4 Disease Cycle.....	12
1.5 Toxins Produced.....	13
2. References for Chapter 2.....	13
Chapter 3: Metabolites.....	16
“Temperature-Induced Metabolic Shifts in <i>Macrophomina phaseolina</i>: A Comparative Study at 28°C and 35°C”.....	16
1. Introduction.....	16
2. Materials and Methods.....	17
2.1 Fungal culture conditions.....	17
2.2 Intracellular Metabolites Extraction.....	17
2.3 Extracellular Metabolites Extraction.....	18
2.4 Derivatization.....	18
2.5 GC-MS conditions.....	19
2.6 Data Pre-processing.....	19
3. Results for ICM.....	25
3.1 PCA Analysis.....	25
3.2 Fold Change Analysis and Volcano Plot.....	26
3.3 OLPS-DA.....	28
3.4 Differentially Expressed Intracellular Metabolites.....	30

4. Results for ECM.....	33
4.1 PCA Analysis.....	33
4.2 Fold Change Analysis and Volcano Plot.....	34
4.3 OLPS-DA.....	36
4.4 Differentially Expressed Extracellular Metabolites.....	37
5. Conclusion.....	40
6. References for Chapter 3.....	40
Chapter 4: The Cell Wall.....	41
“Characterization of <i>Macrophomina phaseolina</i> Cell Wall: Insights into Pathogenicity and Plant Immunity Interactions”.....	41
1. Introduction.....	41
2. Materials and Methods.....	42
2.1 Isolation of Alcohol Insoluble Residue (AIR).....	42
2.2 Preparation of Alkali-insoluble (AKI) and Alkali-Soluble (AKS).....	42
2.3 Processing of the AKS Fraction.....	42
2.4 Processing of the AKI Fraction.....	43
2.5 Monosaccharide Analysis.....	43
2.6 Glycosidic Linkage Analysis.....	43
2.7 Quantification Assays.....	44
2.8 ROS Burst Assay.....	45
3. Results.....	46
3.1 Monosaccharide Analysis.....	46
3.2 Glycosidic Linkage Analysis.....	47
3.3 Quantification Assays.....	48
3.4 ROS Burst Assay.....	50
4. Conclusion.....	51
5. References for Chapter 4.....	51
Conclusion.....	53
Appendix A – EPS.....	54

Isolation Process.....	54
Yield of EPS 28 vs EPS 35.....	54
Deproteinization of EPS.....	55
Appendix B – Publications/Conference Presentations.....	57

List of Figures

- Fig 1:** Disease cycle of *Macrophomina phaseolina*.
- Fig 2:** Yield table recording the wet weight of *Mp* mycelia at 28°C and 35°C.
- Fig 3:** Lyophilized ICM 28 and 35 samples.
- Fig 4:** Density plots for a) ICM and b) ECM data before and after normalization.
- Fig 5:** The original data received after comparison with the NIST database.
- Fig 6:** Final .csv file for ICM data with 65 metabolites in MetaboAnalyst 6.0 format.
- Fig 7:** Scree Plot for ICM with PC1 and PC2 accounting for 72.4% of the variance.
- Fig 8:** PCA Scores Plot for ICM data showing clear separation of both groups.
- Fig 9:** Fold Change (FC=2) Analysis Chart for ICM.
- Fig 10:** Student's t-test for ICM with a confidence level of 95%.
- Fig 11:** Volcano Plot for ICM data showcasing downregulated metabolites in violet and upregulated metabolites in red.
- Fig 12:** The OPLS-DA score plot for ICM data.
- Fig 13:** Values for the OPLS-DA model for ICM.
- Fig 14:** VIP values chart for ICM metabolites.
- Fig 15:** The list of 22 differentially regulated intracellular metabolites.
- Fig 16:** Overview of the enriched metabolic pathways for ICM.
- Fig 17:** Scree Plot for ECM with PC1 and PC2 accounting for 71.6% of the variance.
- Fig 18:** PCA Scores Plot for ECM data showing clear separation of both groups.
- Fig 19:** Fold Change (FC=2) Analysis Chart for ECM.
- Fig 20:** Student's t-test for ECM with a confidence level of 95%.
- Fig 21:** Volcano Plot for ECM data showcasing downregulated metabolites in violet and upregulated metabolites in red.
- Fig 22:** The OPLS-DA Score Plot for ECM data.
- Fig 23:** Reliability metrics for the OLPS-DA model for ECM.
- Fig 24:** VIP values chart for ECM metabolites.
- Fig 25:** The list of 15 differentially regulated extracellular metabolites.
- Fig 26:** Overview of the enriched metabolic pathways for ECM.
- Fig 27:** Yield table recording of AKS/I obtained from AIR.
- Fig 28:** Monosaccharide estimation (%mol) in the different fractions
- Fig 29:** Monosaccharide analysis comparison between the fractions.

Fig 30: Glycosidic linkage estimation (%mol) in the different fractions.

Fig 31: Glycosidic linkage comparison between the fractions

Fig 32: Estimation of a) total sugars, and b) hexoses in the different fractions.

Fig 33: Estimation of uronic acids in the different fractions.

Fig 34: Estimation of chitin in the different fractions.

Fig 35: Graph showing ROS burst for the different fractions.

Fig 36: EPS 28 and EPS 35 after thawing post cryogelation.

Fig 37: Yield table recording the wet weight of *Mp* EPS at 28°C and 35°C.

Fig 38: EPS Deproteinization buffer (500 mL).

Fig 39: My poster for the CARBO-XXXVIII conference.

Abbreviations and Symbols

AIR	Alcohol Insoluble Residues
AKI	Alkali Insoluble
AKS	Alkali Soluble
AKS/I	Alkali Soluble/Insoluble
CW	Cell wall
DMSO	dimethyl sulfoxide
ECM	Extracellular metabolites
EI	Electron ionization
EPS	Extracellular polymeric substances
GC-MS	Gas Chromatography-Mass Spectrometry
ICM	Intracellular metabolites
MeOx	Methoxyamine hydrochloride
<i>Mp</i>	<i>Macrophomina phaseolina</i>
MSTFA	n-methyl-n-trimethylsilyl-trifluoroacetamide
MQ	Milli-Q water
NIST	National Institute of Standards and Technology
PMAA	Permethylated alditol acetates
PTI	Pattern-triggered immunity
ROS	Reactive oxygen species
RT	Room temperature
TFA	Trifluoroacetic acid
m/z	Mass/charge
mL	Millilitre
µL	Microlitre
%	Percentage
<	Less than
>	Greater than
°C	Degree Celsius

Abstract

This thesis compiles my research work on *Macrophomina phaseolina* (*Mp*), a necrotrophic heat- and drought-favouring fungal pathogen responsible for significant crop losses. The thesis itself is divided into two major sections. The first section investigates the temperature-induced metabolic shifts in *Mp* at 28°C and 35°C through untargeted GC-MS. By analyzing both intracellular and extracellular metabolites, potential biomarkers, such as Xylitol and 3,4,8-Trihydroxycoumarin, were identified for the heat stress condition. This study sheds light on the pathogen's differential metabolomic profiles across varying temperatures.

The second section characterizes *Mp*'s cell wall (CW) composition. Monosaccharide and glycosidic linkage profiling revealed that different fractions of the cell wall (CW) possess distinct compositional profiles, which suggested varying immunogenic potentials. This hypothesis was then tested by analyzing early pattern-triggered immunity (PTI) markers, such as the transient ROS burst. The study reveals significant differences in CW components that may elicit differential immune responses in plant systems. We also quantify the total sugars, hexoses, uronic acids, and chitin content of the CW fractions for a deeper insight into their compositions.

The findings provide critical insights into the pathogenicity of *Mp* and its interactions with host plants such as Soybean (*Glycine max*), contributing to the growing field of research for the development of strategies to mitigate the effect of this pathogen under changing climatic conditions.

Chapter 1: Introduction

The charcoal rot pathogen *Macrophomina phaseolina* (*Mp*) is a deadly necrotrophic soil-borne fungus, infecting more than 500 plant species in more than 100 families worldwide, including several commercially important crops such as soybean, sorghum, and maize.

This soil-dwelling pathogen can infect soybean (the chosen host organism for this study), at any stage of crop development, although infection typically occurs during the post-flowering period. Changed weather patterns, i.e. increases in temperatures, erratic rainfall patterns, and lengthier drought conditions, have favored the spread and impact of this pathogen and have become a severe disease in India, a minor disease until 2004 (Yang et al., 2023). Although this pathogen is capable of causing severe disease under a variety of environmental conditions, it is a heat- and drought-favoring disease, and with rising global temperatures, it poses a serious threat to crop loss and global food security.

The following objectives for my thesis guide the investigation of this fungi into its biological and biochemical aspects to understand what contributes to its enhanced pathogenicity:

1. To investigate the temperature-induced metabolic shifts in *Macrophomina phaseolina* (*Mp*) at 28°C and 35°C, aiming to identify potential biomarkers by analyzing differentially expressed intracellular and extracellular metabolites.
2. To characterize the cell wall composition of *Mp* by isolating its alcohol-insoluble residues and studying the key monosaccharides, glycosidic linkages, and quantifying general sugars, hexoses, uronic acids, and chitin.
3. To assess the immunogenic potential of *Mp* cell wall fractions by evaluating immune responses in host plant leaf systems, using early pattern-triggered immunity (PTI) markers.

The thesis henceforth has been organized into distinct chapters to provide a clear structure. Each chapter is dedicated to a specific project undertaken during this research. The chapters are outlined as follows:

Chapter 2 presents a review of the available literature relevant to different aspects of the present investigation.

Chapter 3, titled “Metabolites,” provides a comprehensive study on the temperature-induced metabolic shifts in *Macrophomina phaseolina* (*Mp*). Using untargeted metabolomics via GC-MS, this study investigates intracellular and extracellular metabolites at 28°C and 35°C, uncovering how elevated temperatures amplify pathogenicity. The chapter discusses the procedural rigor behind metabolite

extraction, data preprocessing, and analytical approaches such as PCA and OPLS-DA. The results reveal distinct metabolic profiles across the two conditions, identifying potential metabolic markers like Xylitol and 3,4,8-Trihydroxycoumarin, which exhibit significant temperature-dependent expression patterns. This chapter establishes a foundational understanding of *Mp*'s metabolic adaptations under thermal stress, paving the way for targeted interventions in crop protection.

In Chapter 4, we explore the composition and immunogenic properties of the *Mp* cell wall (CW), an essential structure contributing to its pathogenicity. We conducted a detailed analysis of the CW fractions, including their monosaccharide composition, glycosidic linkage profile, and several quantification assays estimating the total sugars, hexoses, uronic acids, and chitin content. This chapter also investigates the differential immunogenic responses of these fractions in host plant leaves.

References for Chapter 1

Yang, L., Song, W., Xu, C., Sapey, E., Jiang, D., & Wu, C. (2023). Effects of high night temperature on soybean yield and compositions. *Frontiers in Plant Science*, 14. <https://doi.org/10.3389/fpls.2023.1065604>

Chapter 2: Review of Literature

1.1 Introduction

Macrophomina phaseolina (Tassi) Goid is a necrotrophic, soil-borne fungal pathogen belonging to Kingdom Fungi, Phylum Ascomycota, Class Dothideomycetes, Order Botryosphaerales, and Family Botryosphaerales. Despite being predominantly recognized as a necrotrophic pathogen, a study by Chowdhury et al. (2017) revealed an intriguing biotrophic phase during the early stages of infection in soybean. This biotrophic phase, which lasts up to 36 hours, is then followed by a shift to necrotrophy.

1.2 Host Range and Economic Importance

Macrophomina phaseolina has an extensive host range, infecting over 500 species across 100 plant families (Su et al., 2001). Prominent global crops, such as alfalfa, canola, sunflower, maize, sesame, and soybean are among its hosts (Gaétan et al., 2006; Saleh et al., 2010). In addition, crops like chickpea, mungbean, and cassava, that are important for regional food security in India, are also vulnerable to this pathogen. (Ammon et al., 1974; Bashir & Malik, 1988; Kaiser & Das, 1988; Weems et al., 2011; Lakhran et al., 2018).

The pathogen's impact is exacerbated under heat and drought stress conditions. *Mp* can significantly reduce crop yields and threaten food security for crops such as soybean and sorghum which are traditionally already grown in places where the soil moisture content is low, and temperatures are high (30-35°C) (Dhillon et al., 2012). For instance, pre-emergence infections by this fungus have been reported to cause 100% yield losses in groundnut cultivars (Sharma & Bhowmik, 1986). Such sweeping losses highlight the impact of this pathogen on agricultural output and farmers' livelihoods (Kaur et al., 2012).

1.3 Morphological Characteristics

The ability of *Macrophomina phaseolina* to persist in unfavorable conditions can partially be attributed to the production of microsclerotia, which are dark-colored asexual propagation structures. These enable the fungi to survive in the soil for several years without requiring a host, making it challenging to eradicate it from infected fields.

Microscopically, *Mp* exhibits hyaline hyphae with thin walls that transition to light or dark brown hyphae with septa. Branches often originate at right angles from the parent hyphae and constrict at the point of origin (Lakhran et al., 2018). Under natural conditions, pycnidia formation is rare. When observed, these structures are

black, rough, irregular, and significantly larger than microsclerotia (Lakhran et al., 2018). The morphological heterogeneity of this fungi—reflected in the variations in mycelial color, microsclerotia distribution, and pycnidia formation—is influenced by environmental factors (Tok, 2019; Pandey et al., 2020) and contributes to be a challenge for researchers working on infection mitigation strategies worldwide.

1.4 Disease Cycle

The primary infectious source of *Mp* is its microsclerotia, which are highly resistant structures capable of surviving in the soil for up to 15 years (Gupta et al., 2012). During favorable conditions, typically between 30 and 35°C, these microsclerotia germinate to produce germ tubes. The germ tubes form specialized structures called appressoria, which penetrate the host epidermis. Once inside the host roots, the fungus disrupts the vascular system, which cuts off the upper section of the plant from receiving nutrients and water. This disruption leads to the characteristic symptoms of charcoal rot disease such as wilting and a gray discoloration of stem tissues due to the accumulation of microsclerotia.

As the disease advances, symptoms manifest as yellowing and premature senescence of leaves, which remain attached to the stems by petioles. The cortical tissues of the lower stem and taproot slough off, exposing gray tissues laden with microsclerotia. In severe cases and under conducive high stress environmental conditions, the host plant prematurely dies (Short et al., 1978). The disease cycle perpetuates when infected root and stem debris are returned to the soil, where the microsclerotia will persist or initiate new infections.

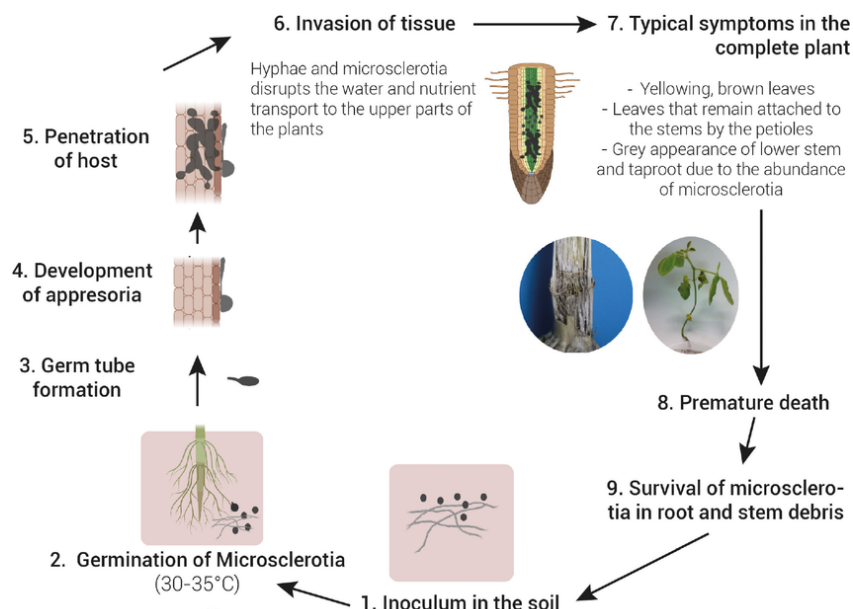


Fig 1: Disease cycle of *Macrophomina phaseolina*

1.5 Toxins Produced

Macrophomina phaseolina has been reported to produce more than a dozen mycotoxins and other secondary metabolites (Khambhati et al., 2020), including phaseolinone, mellein, phaseolinic acid and (–)-botryodiplodin (Dhar et al., 1982; Mahato et al., 1987; Ramezani et al., 2007; Bhattacharya et al., 1992; Masi et al., 2021; Abbas et al, 2019). However, the complete metabolomic profile of *Mp* under varying environmental conditions remains inadequately studied.

The exact mechanism by which *Mp* infect plants with charcoal rot disease is not yet understood, which is partly due to the genetic and phenotypic diversity observed among isolates of the fungus (Nakagawa et al., 1979; Bladt et al., 2013; McCurry et al., 1973; Moule et al., 1981). Nonetheless, it has been theorized that toxins produced by this fungus can play a critical role in the early stages of infection, essentially allowing the pathogen to establish itself from the soil reservoir, where it can survive adverse conditions, particularly during winter (Bellaloui et al., 2021; Moule et al., 1984).

2. References for Chapter 2

1. Chowdhury, S., Basu, A., & Kundu, S. (2017). Biotrophy-necrotrophy switch in pathogen evoke differential response in resistant and susceptible sesame involving multiple signaling pathways at different phases. *Scientific Reports*, 7(1). <https://doi.org/10.1038/s41598-017-17248-7>
2. Su, G., Suh, S., Schneider, R. W., & Russin, J. S. (2001). Host Specialization in the Charcoal Rot Fungus, *Macrophomina phaseolina*. <https://doi.org/10.1094/phyto.2001.91.2.120>
3. Gaetán, S. A., Fernandez, L., & Madia, M. (2006). Occurrence of Charcoal Rot Caused by *Macrophomina phaseolina* on Canola in Argentina. *Plant Disease*, 90(4), 524. <https://doi.org/10.1094/pd-90-0524a>
4. Ammon, V., Wyllie, T. D., & Brown, M. F. (1974). An ultrastructural investigation of pathological alterations induced by *Macrophomina phaseolina* (Tassi) Goid in seedlings of soybean, *Glycine max* (L.) Merrill. *Physiological Plant Pathology*, 4(1), 1–4. [https://doi.org/10.1016/0048-4059\(74\)90038-1](https://doi.org/10.1016/0048-4059(74)90038-1)
5. Bashir, M., & Malik, B. A. (1988). Diseases of major pulse crops in Pakistan—a review. *Tropical Pest Management*, 34(3), 309–314. <https://doi.org/10.1080/0967087880937126>
6. Kaiser, S. a. K. M., & Das, S. N. (1988). Physical Factors that Influence the Growth and Spread of Charcoal Rot Pathogen (*Macrophomina phaseolina*) Infecting Maize. *Journal of Phytopathology*, 123(1), 47–51. <https://doi.org/10.1111/j.1439-0434.1988.tb01035.x>

7. Weems, J. D., Ebelhar, S. A., Chapara, V., Pedersen, D. K., Zhang, G. R., & Bradley, C. A. (2011). First Report of Charcoal Rot Caused by *Macrophomina phaseolina* on Sunflower in Illinois. *Plant Disease*, 95(10), 1318. <https://doi.org/10.1094/pdis-02-11-0102>
8. Lakhran, L., Ahir, R., Choudhary, M., & Choudhary, S. (2018). Isolation, purification, identification and pathogenicity of *macrophomina phaseolina* (Tassi) goid caused dry root rot of chickpea. *Journal of Pharmacognosy and Phytochemistry*, 7(3), <https://www.phytojournal.com/archives/2018/vol7issue3/PartAS/7-3-442-786.pdf> 3314–3317.
9. Kaur, S., Dhillon, G. S., Brar, S. K., Vallad, G. E., Chand, R., & Chauhan, V. B. (2012). Emerging phytopathogen *Macrophomina phaseolina*: biology, economic importance and current diagnostic trends. *Critical Reviews in Microbiology*, 38(2), 136. <https://doi.org/10.3109/1040841x.2011.640977>
10. Sharma, R. C., & Bhowmik, T. P. (1986). Estimation of yield losses in groundnut due to *Macrophomina phaseolina* (Tassi) Goid. *Indian Journal of Plant Pathology*, 4(2), 108-112.
11. Tok, F. M. (2019). Relationship between morphologic, phenotypic and pathogenic characteristics in *Macrophomina phaseolina* Isolates from cucumber plants. *Int. J. Innov. Approaches Agric. Res.*, 3, 651-660.
12. Gupta, G. K., Sharma, S. K., & Ramteke, R. (2012b). Biology, Epidemiology and Management of the Pathogenic Fungus *Macrophomina phaseolina* (Tassi) Goid with Special Reference to Charcoal Rot of Soybean (*Glycine max* (L.) Merrill). *Journal of Phytopathology*, 160(4), 167–180. <https://doi.org/10.1111/j.1439-0434.2012.01884.x>
13. Short, G. E., Wyllie, T. D., and Ammon, V. D. (1978). Quantitative enumeration of *Macrophomina phaseolina* in soybean tissues. *Phytopathology* 68, 736–741.
14. Marquez, N., Giachero, M. L., Declerck, S., & Ducasse, D. A. (2021). *Macrophomina phaseolina*: General Characteristics of Pathogenicity and Methods of Control. *Frontiers in Plant Science*, 12. <https://doi.org/10.3389/fpls.2021.634397>
15. Khambhati V.H., Abbas H.K., Sulyok M., Tomaso-Peterson M., Shier W.T. First report of the production of mycotoxins and other secondary metabolites by *Macrophomina phaseolina* (Tassi) Goid. isolates from soybeans (*Glycine max* L.) symptomatic with charcoal rot disease. *J. Fungi.* 2020;6:332. doi: 10.3390/jof6040332.
16. Dhar T.K., Siddiqui K.A.I., Ali E. Structure of phaseolinone, a novel phytotoxin from *Macrophomina phaseolina*. *Tetrahedron Lett.* 1982;23:5459–5462.
17. Mahato S.B., Siddiqui K.A.I., Bhattacharya G., Ghosal T., Miyahara K., Sholichin M., Kawasaki T. Structure and stereochemistry of phaseolinic acid: A new acid from *Macrophomina phaseolina*. *J. Nat. Prod.* 1987;50:245–247. doi: 10.1021/np50050a024.

18. Ramezani M., Shier W.T., Abbas H.K., Tonos J.L., Baird R.E., Sciumbato G.L. Soybean charcoal rot disease fungus *Macrophomina phaseolina* in Mississippi produces the phytotoxin (–)-botryodiplodin but no detectable phaseolinone. *J. Nat. Prod.* 2007;70:128–129. doi: 10.1021/hp060480t.
19. Bhattacharya D., Dhar T.K., Ali E. An enzyme immunoassay of phaseolinone and its application in estimation of the amount of toxin in *Macrophomina phaseolina*-infected seeds. *Appl. Environ. Microbiol.* 1992;58:1970–1974. doi: 10.1128/aem.58.6.1970-1974.1992.
20. Masi M., Sautua F., Zatout R., Castaldi S., Arrico L., Istituto R., Pescitelli G., Carmona M.A., Evidente A. Phaseocyclopentenones A and B, phytotoxic penta- and tetrasubstituted cyclopentenones produced by *Macrophomina phaseolina*, the causal agent of charcoal rot of soybean in Argentina. *J. Nat. Prod.* 2021;84:459–465. doi: 10.1021/acs.jnatprod.0c01287.
21. Abbas H., Bellaloui N., Accinelli C., Smith J.R., Shier W.T. Toxin production in soybean (*Glycine max* L.) plants with charcoal rot disease and by *Macrophomina phaseolina*, the fungus that causes the disease. *Toxins.* 2019;11:645. doi: 10.3390/toxins11110645.
22. Nakagawa F., Kodama K., Furuya K., Naito A. New strains of botryodiplodin producing fungi. *Agric. Biol. Chem.* 1979;43:1597–1598. doi: 10.1080/00021369.1979.10863669.
23. Bladt T.T., Frisvad J.C., Knudsen P.B., Larsen T.O. Anticancer and antifungal compounds from *Aspergillus*, *Penicillium* and other filamentous fungi. *Molecules.* 2013;18:11338–11376. doi: 10.3390/molecules180911338.
24. McCurry P.M., Abe K. Stereochemistry and synthesis of the antileukemic agent botryodiplodin. *J. Am. Chem. Soc.* 1973;95:5824–5825. doi: 10.1021/ja00798a097.
25. Moule Y., Decloitre F., Hamon G. Mutagenicity of the mycotoxin botryodiplodin in the *Salmonella typhimurium*/ microsomal activation test. *Environ. Mutagenesis.* 1981;3:287–291. doi: 10.1002/em.2860030311.
26. Bellaloui N., Mengistu A., Smith J.R., Abbas H.K., Accinelli C., Shier W.T. Effects of charcoal rot on soybean seed composition in soybean genotypes that differ in charcoal rot resistance under irrigated and non-irrigated conditions. *Plants.* 2021;10:1801. doi: 10.3390/plants10091801.
27. Moule Y., Darracq N. Absence of DNA breaks during repair of DNA-protein cross-links induced by the mycotoxin botryodiplodin in mammalian cells. *Carcinogenesis.* 1984;5:1375–1377. doi: 10.1093/carcin/5.10.1375.

Chapter 3: Metabolites

“Temperature-Induced Metabolic Shifts in *Macrophomina phaseolina*: A Comparative Study at 28°C and 35°C”

1. Introduction

In this study, we explore the metabolomic changes that occur in *Macrophomina phaseolina* (*Mp*) when grown at two distinct temperatures: 28°C and 35°C. It is hypothesized that *Mp* induces local necrosis in plant roots by releasing toxins (Khambhati et al., 2023), a strategic mechanism that not only weakens host defenses but also facilitates the fungi's entry and colonization, ultimately establishing a successful infection. This makes *Mp*'s extracellular metabolites a particularly interesting area of exploration, offering a window into the biochemical arsenal utilized by this fungi to establish infection, disrupt host defenses, and facilitate its entry into plant tissues.

Additionally, the pathogenicity of *Mp* is reported to increase with temperature, resulting in more severe symptoms in the host (Basandrai et al., 2021). Although *Mp*-produced toxins such as mellein (Khambhati et al., 2023) and botryodiplodin (Alam et al., 2022) have been characterized earlier, comprehensive metabolic profiling across varying temperatures has not yet been explored. By investigating the metabolic shifts between 28°C and 35°C, this study aims to uncover the biochemical drivers of the fungi's enhanced pathogenicity at higher temperatures.

This research is particularly important at a time when mean annual soil temperatures continue to rise globally due to climate change. A Nature 2023 study revealed that soil heat extremes outpace air temperature extremes by 0.7°C per decade in intensity and occur twice as fast in frequency (Almudena García-García et al., 2023). The insights from this study would also allow for the targeted analysis of the metabolites involved in plant-fungal interactions and ultimately contribute to the development of resistant crop varieties to mitigate the disease's impact. This project thus fills a critical knowledge gap in fungal metabolomics and forms the basis of my undergraduate thesis.

By employing untargeted metabolomics to profile the exo- and endo-metabolomic changes in *Mp* at 28°C and 35°C through GC-MS, we aimed to identify and compare the intracellular and extracellular metabolites being produced by the fungi under these differential temperature conditions, to study the changes in the core metabolic functions within the fungal cells, and the differential secreted metabolic byproducts of the fungal culture respectively.

2. Materials and Methods

2.1 Fungal culture conditions

Fungal mycelia were grown in Potato Dextrose Broth (PDB) medium at 28°C and 35°C and collected after an incubation period of three days. Approximately 200ml of the culture media was filtered using a Mira cloth to separate the mycelia. Agar plugs were removed, and the mycelia was thoroughly washed twice with MQ to ensure that all extracellular polymeric substances (EPS) were removed.

Excess water was squeezed out of Mira cloth, and the wet weight of the mycelia per 200 mL culture was recorded, averaging around ~25 g at 28°C and ~15g at 35°C, resulting in a yield ratio of 4.9:1 for 28°C to 35°C cultures.

	Grams (per 200 mL culture)	
	Myc 28	Myc 35
R1	26.67	15.59
R2	22.99	16.20
R3	25.88	14.32
Avg	25.18	15.37

Fig 2: Yield table recording the wet weight of *Mp* mycelia at 28°C and 35°C.

2.2 Intracellular Metabolites Extraction

For each biological replicate, 15 grams of mycelia was accurately weighed, to which 30 ml of the extraction solvent (acetonitrile:water = 1:1, v/v) was added. The mixture was sonicated at 30°C for 5 minutes to disrupt the mycelial mass. A freeze-thaw cycle was then performed by freezing the samples in liquid nitrogen and subsequently thawing them at 28°C for 24 hours to facilitate cell lysis. Following thawing, samples were vortexed briefly to ensure homogeneity and centrifuged at 12,000 RPM at room temperature for 20 minutes. The supernatant (6 mL) was carefully collected without disturbing the pellet. This supernatant was lyophilized until a powder was obtained.



Fig 3: Lyophilized ICM 28 and 35 samples.

The dried samples were reconstituted by adding 1 ml of acetonitrile using glass pipette tips to prevent plastic contamination. The reconstituted mixture was vortexed, followed by another round of centrifugation. From the final supernatant, 200 μ L was collected and designated as the sample of interest for derivatization. Before derivatization, the acetonitrile was evaporated under a nitrogen stream at 30°C for 10 minutes.

2.3 Extracellular Metabolites Extraction

Extracellular metabolites were extracted using a 2:5:2 ratio mixture of chloroform, methanol, and water, respectively. Culture filtrates for both 28°C and 35°C samples were centrifuged, and 2 mL of each replicate was aliquoted into 15 mL falcon tubes. To each aliquot, an equal volume of C:M:W (2:5:2) was added, followed by gentle vortexing. Samples were incubated at 28°C overnight to allow for phase separation. After incubation, the samples were centrifuged to separate the aqueous and organic phases. From each sample, 1 mL of both the aqueous and organic phases was transferred into separate Pyrex tubes. These aliquots were then lyophilized to dryness and considered for derivatization.

2.4 Derivatization

Methoximation was performed by adding 80 μ L of methoxyamine hydrochloride (MeOx) solution (20 mg/mL in pyridine) to each sample, followed by incubation at 30°C for 2 hours. Silylation was subsequently carried out by adding 100 μ L of N-methyl-N-(trimethylsilyl) trifluoroacetamide (MSTFA) and incubating at 37°C for 2

hours. The fully derivatized samples were transferred to GC-MS-appropriate glass vials, and 2 μ L of each sample was injected into the GC-MS system for analysis.

2.5 GC-MS conditions

GC-MS for both ICM and ECM samples were conducted on a 30 m \times 0.25 mm Rxi-5Sil MS Column. Helium flow was 1 mL min $^{-1}$ with splitless injection.

For ICM, injection was made at 60°C with a 1-min hold, after which the temperature was ramped up to 180°C at 10°C min $^{-1}$, and then to 300°C at 4°C min $^{-1}$, with a 10-min hold at the highest temperature. The total program time was thus 55 minutes.

For ECM, the injection was made at 90°C, and then temperature was ramped to 180°C at 10°C min $^{-1}$, followed by a rise to 240°C at 5°C min $^{-1}$, and then to 290°C at 25°C min $^{-1}$ with no holds at any of the temperatures. Thus, the total program time was only 23 minutes.

The original GC-MS data was automatically identified by comparing them to the National Institute of Standards and Technology (NIST) database. The identification is made by comparing the EI mass spectrometry fragments of the detected metabolites to what is stored in the database.

2.6 Data Pre-processing

For further analysis, a metabolite was considered relevant if it was present in at least two out of the three replicates for a particular temperature. Hits with a similarity index of 70 or higher to NIST were considered. Metabolites were compared based on the area under the peak.

The data was normalized using the median, followed by log10 transformation. Data scaling was performed through Pareto scaling (in which the data were mean-centered and divided by the square root of the standard deviation). This preprocessing ensured that metabolite signals with subtle but meaningful changes could be detected without being overshadowed by few extreme values. The resulting data matrix was then exported to MetaboAnalyst 6.0 for further analysis.

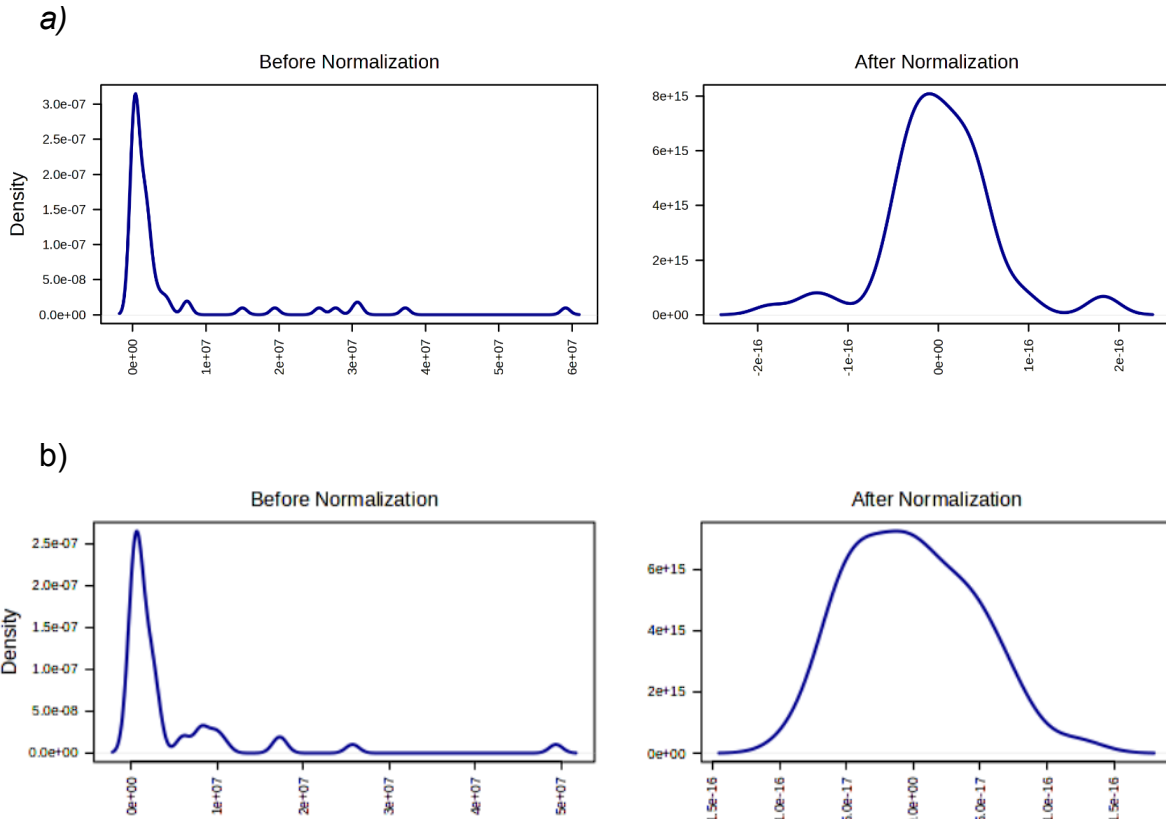


Fig 4: Density plots for a) ICM and b) ECM data before and after normalization. The x-axis represents the peak intensities, and the y-axis represents the probability density of finding metabolites with a given intensity value. Raw intensities (left) are heavily skewed towards low values, while normalized intensities (right) follow a symmetric distribution after log transformation and Pareto scaling.

2.6.1 Data Analysis for Intracellular Metabolites (ICM)

Data analysis for ICM involved processing seven samples, with three replicates per group and one blank. The compounds identified from the blank were removed from the other six samples of interest. Finally, out of the ~100 identified compounds, the final dataset was refined to include 65 metabolites formatted for MetaboAnalyst 6.0.

Compound Name	RT	m/z	Area	Height	SI
Silane, chlorotrimethyl-	0	1.78	0 Target	9549072101 8175185 ppm	0 Auto(Saturation)
2-isopropenyl-3,6-dimethylpyr* Ratio of reference ion does not match.	0	0 Target	148	0 ppm	0 Auto
1,2-Butanediol, 2TMS derivative*	0	2.191	0 Target	14942676798 6100337 ppm	0 Auto(Saturation)
1,2-Butanediol, 2TMS derivative* Ratio of reference ion does not match.	0	0 Target	131	0 ppm	0 Auto
Sulfurous acid, dimethyl ester Ratio of reference ion does not match.	0	0 Target	79	0 ppm	0 Auto
Tetrahydrofuran-08	0	2.59	0 Target	8013230051 1480350 ppm	0 Auto(Saturation)
N-Methyltrifluoroacetamide, TIP* Ratio of reference ion does not match.	0	0 Target	184	0 ppm	0 Auto
Methylyamine, 2TMS derivative	0	4.149	0 Target	16040592462 7070293 ppm	0 Auto(Saturation)
Methylyamine, 2TMS derivative	0	4.26	0 Target	16033428266 5884845 ppm	0 Auto
2,2,2-Trifluoroethane-1,1-diol, P* Ratio of reference ion does not match.	0	0 Target	147	0 ppm	0 Auto
Methoxyamine, 2TMS derivative*	0	4.965	0 Target	19142705730 8391236 ppm	0 Auto(Saturation)
Dimethylane, hexamethyl-	0	5.156	0 Target	7332442973 1405348 ppm	0 Auto(Saturation)
N-tert-butyltrimethylsilyl)-2,2,2*	0	5.393	0 Target	772237966 1177369 ppm	0 Auto
Lactic Acid, 2TMS derivative	0	6.391	0 Target	1471268031 482298 ppm	0 Auto
Diglycolic acid, 2TMS derivative Ratio of reference ion does not match.	0	6.971	0 Target	147388468 196790 ppm	0 Auto
Tris(trimethylsilyl)carbamate	0	7.583	0 Target	14714975049 5555315 ppm	0 Auto
1-(Trimethylsilyl)-3-[(Trimethylsilyl) Pentadioxane, heptadecane-thi-	0	7.952	0 Target	371366402 172181 nm	0 Auto

Fig 5: The original data received after comparison with the NIST database.

Sample	28_R1	28_R2	28_R3	35_R1	35_R2	35_R3
Label	28	28	28	35	35	35
1	2494094	123673	2115479	1731366	2299477	1278848
2	328564	0	0	0	0	0
3	2858675	3748241	2036726	1272235	1571031	809889
4	0	0	0	742626	512866	478331
5	170145	0	389505	0	0	0
6	3379016	4494862	0	0	0	0
7	531170	453433	345763	0	0	0
8	1490634	1114488	916195	4164277	3945274	2712659
9	1021739	1964152	1274334	1848102	2271705	2060684
10	4455531	8024762	5074809	2694552	4633865	2107165
11	280549	118924	508736	219817	212874	0
12	0	1303679	0	0	0	0
13	1561461	1124657	964643	6645064	4720252	5598306
14	0	0	0	382871	306371	0
15	333245	339680	0	2231469	831389	0
16	0	0	475398	0	0	2455208
17	0	0	0	0	952585	436716
18	293543	0	0	0	0	0
19	0	0	0	144364	703874	311009
20	940982	1578169	1343776	1398463	2220805	1166331

Fig 6: A glimpse of the final .csv file for ICM data containing 65 metabolites in MetaboAnalyst 6.0 format. Compound names were stored in a separate sheet corresponding to the labels 1-65 shown in column A.

2.6.2 Data Analysis for Extracellular Metabolites (ECM)

Data analysis for ECM was similar to ICM with the difference that the upper and lower phases for each replicate collected after the C:M:W extraction method were compared separately for 28°C and 35°C, after which the data for differentially expressed metabolites were pooled. The final dataset included a total of 50 metabolites submitted for analysis on MetaboAnalyst 6.0.

2.6.3 Scripts Useful for Analysis

Some R scripts were written whenever required to make the data cleaning work easier. Putting them below for reference.

Script 1: Removing Specific Columns Across All Sheets in an Excel Workbook

Description: This R script processes an Excel workbook by extracting specified columns from all sheets and saving the filtered data into a new workbook, ensuring consistent data formatting for analysis.

```
# Load the required package
library(openxlsx)
```

```

# Define the columns to keep (1-based indexing)
columns_to_keep <- c(1, 3, 5, 6, 7, 12) # Example: A, C, E, F, G,
M

# Specify the input and output file paths
input_file <- "path/to/your/input/data.xlsx"
output_file <- "path/to/your/output/filtered_data.xlsx"

# Read the workbook
wb <- loadWorkbook(input_file)

# Get the names of all sheets in the workbook
sheet_names <- names(wb)

# Initialize a list to hold the filtered data for each sheet
all_filtered_data <- list()

# Loop through each sheet and filter the columns
for (sheet_name in sheet_names) {
  # Read the data from the current sheet
  sheet_data <- read.xlsx(input_file, sheet = sheet_name)

  # Keep only the specified columns
  filtered_data <- sheet_data[, columns_to_keep]

  # Add the filtered data to the list
  all_filtered_data[[sheet_name]] <- filtered_data
}

# Write the filtered data to the output file (create the file with
# the first sheet)
write.xlsx(all_filtered_data, output_file)

cat("Filtered workbook saved as", output_file, "\n")

```

Script 2: Filtering Data Based on Replicate Detection in Groups

Description: This R script replaces missing values with zeros for specified columns, then filters rows where detection occurs in at least two replicates within either of two groups. The cleaned dataset is saved to a CSV file for downstream analysis.

```

# Install and load the required packages
install.packages("tidyverse")
install.packages("openxlsx") # For writing to Excel

```

```

library(tidyverse)
library(openxlsx)

# File paths
input_file <- "C:/path to input file/input.csv"
output_file <- "C:/path to output file/output.xlsx"

# Load the data from the CSV file
data <- read_csv(input_file)

# Filter rows where at least 2 of the 3 columns have non-zero
values
filtered_data <- data %>%
  rowwise() %>%
  filter(
    sum(c_across(c('35CF', '35CF2', '35CF3'))) != 0) >= 2
  ) %>%
  ungroup() # Ungroup after rowwise operation

# Print the filtered data
print(filtered_data)

# Write the filtered data to the specified Excel file
write.xlsx(filtered_data, output_file)

cat("Filtered data saved to", output_file, "\n")

```

Script 3: Filter Rows in multiple Excel Sheets Based on a Threshold of ≥ 70

Description: This R script filters rows in multiple sheets of an Excel workbook, keeping only those where the third column value is ≥ 70 and excluding NA values. The filtered data is saved into a new Excel file for further analysis.

```

# Load the required package
library(openxlsx)

# Specify the input and output file paths
input_file <- "C:/path to input file/input.xlsx"
output_file <- "C:/path to output file/output.xlsx"

# Read the workbook
wb <- loadWorkbook(input_file)

```

```

# Get the names of all sheets in the workbook
sheet_names <- names(wb)

# Initialize a list to hold the filtered data for each sheet
all_filtered_data <- list()

# Loop through each sheet and filter the rows based on the third
# column
for (sheet_name in sheet_names) {
  # Read the data from the current sheet without column names
  sheet_data <- read.xlsx(input_file, sheet = sheet_name, colNames
= FALSE)

  # Filter rows where the third column is >= 70
  filtered_data <- sheet_data[!is.na(sheet_data[[3]])] &
  sheet_data[[3]] >= 70, ]

  # Add the filtered data to the list
  all_filtered_data[[sheet_name]] <- filtered_data
}

# Write the filtered data to the output file
write.xlsx(all_filtered_data, output_file)

cat("Filtered workbook saved as", output_file, "\n")

```

3. Results for ICM

This section covers the analysis of results for intracellular metabolites.

3.1 PCA Analysis

The PCA score plot displays samples in a reduced dimensional space, with clustered samples being more similar and samples far apart being more different. The PC1 (principle component 1) and PC2 (principle component 2) explained 54.3% and 18.1% of the variance in the ICM data, respectively, together covering up 72.4% of the variance.

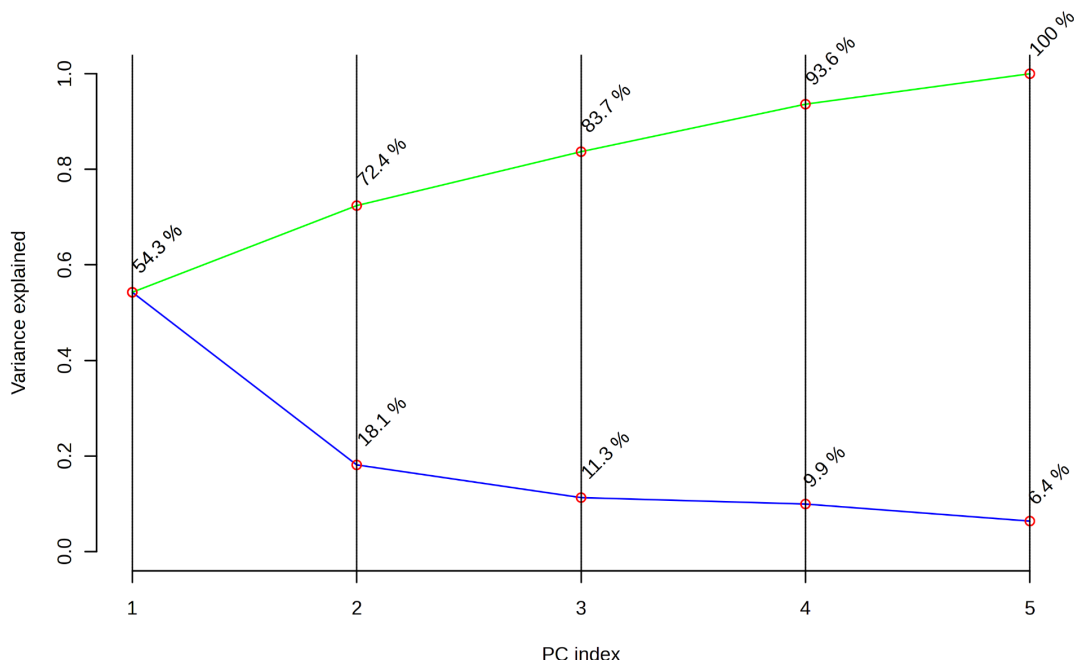


Fig 7: Scree Plot for ICM with PC1 and PC2 accounting for 72.4% of the variance.

Since PC1 accounts for a larger percentage of the variance (54.3%) compared to PC2 (18.1%), an equivalent distance along the x-axis represents a more significant separation than the same distance along the y-axis. Additionally, being an unstructured technique, it shows the main structure of the data without considering a special direction. We already see that the scores plot demonstrates a clear distinction between the replicates of both temperatures, with 28°C clustering on the left and 35°C on the right, all contained within the shaded region representing a 95% confidence interval. This suggests that temperature induces significant variations in intracellular metabolism.

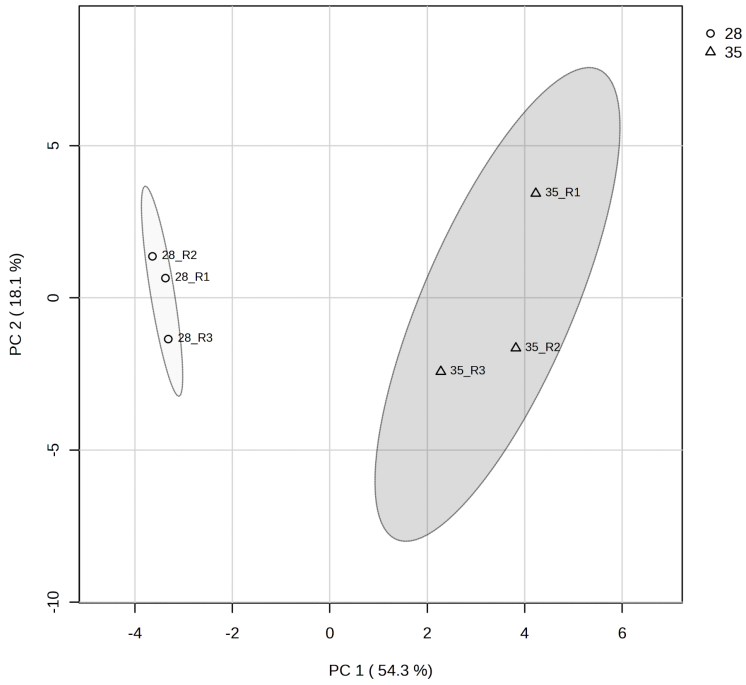


Fig 8: PCA Scores Plot for ICM data showing clear separation of both groups.

3.2 Fold Change Analysis and Volcano Plot

Fold change (FC) analysis compares the absolute values of change between two group means. Taking a significant threshold of 2.0 between 28°C and 35°C, we got 22 significantly downregulated metabolites and 24 significantly upregulated metabolites.

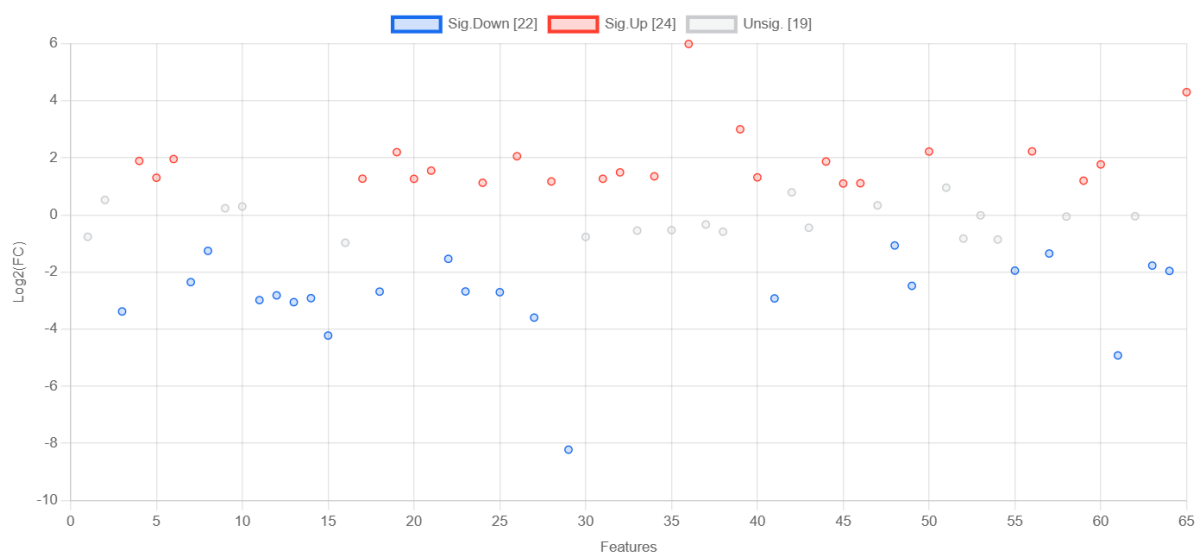


Fig 9: Fold Change (FC=2) Analysis Chart for ICM.

Student's t-test was also performed to compare the features between the two groups. Using a significance threshold of $p < 0.05$, 22 features were identified as statistically significant, while the remaining 43 features were deemed non-significant.

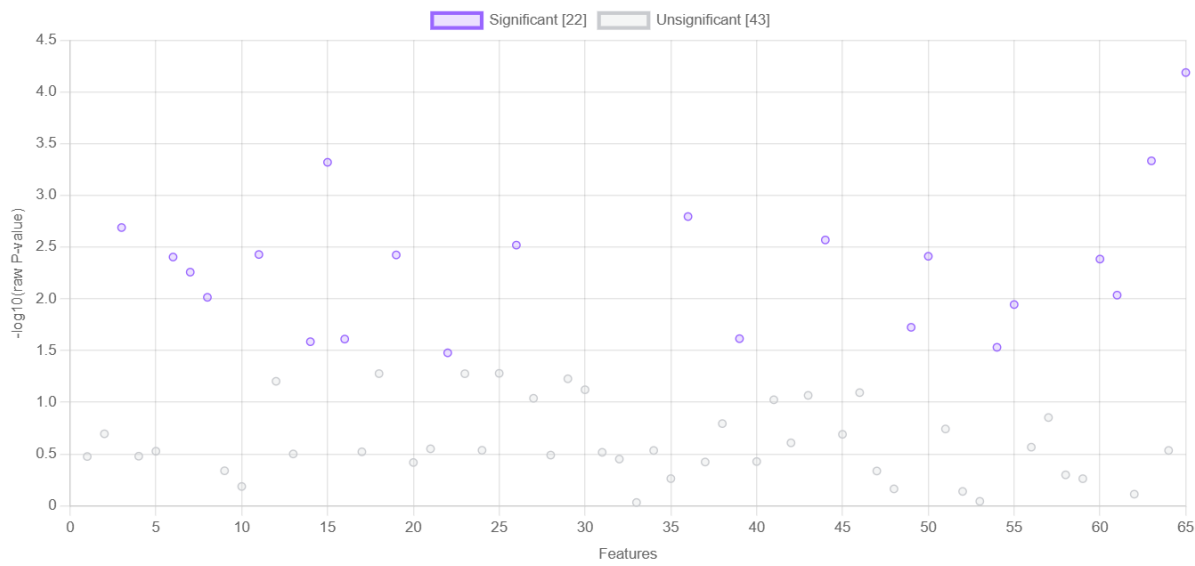


Fig 10: Student's t-test with a confidence level of 95% gives us 22 significant intracellular metabolites.

Volcano plots enable quick visual identification of the most meaningful features between two conditions by combining both fold change and statistical significance.

In this plot, fold change is represented on the x-axis, while the negative log10 of the p-value is plotted on the y-axis. Metabolites with positive fold changes are highlighted in red, while those with negative fold changes are shown in violet, with the point size representing the significance level.

The horizontal dashed black line indicates the threshold for $p = 0.05$, with points above the line indicating significant features ($p < 0.05$) and points below it indicating non-significant features ($p > 0.05$). The two vertical dashed black lines represent $FC = 2$ and $FC = -2$, and features outside these lines with $p < 0.05$ are considered to be significant. Only significant metabolites have been numbered.

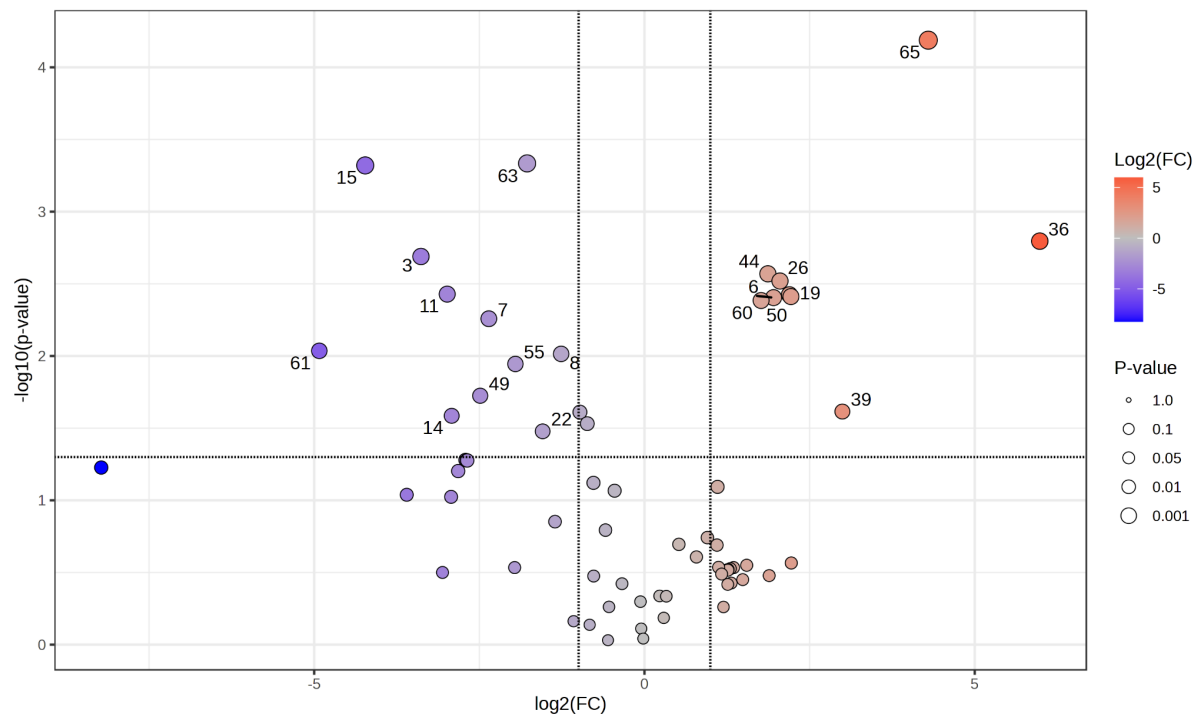


Fig 11: Volcano Plot for ICM data showcasing downregulated metabolites in violet and upregulated metabolites in red.

3.3 OLPS-DA

OPLS-DA (Orthogonal Partial Least Squares Discriminant Analysis) is used to separate the variation in data into predictive and orthogonal components, helping to distinguish between different groups while minimizing noise. Here, the advantage is that the between-group variation (class separation) is seen in the first component, and the within-group variation will be seen in the orthogonal components.

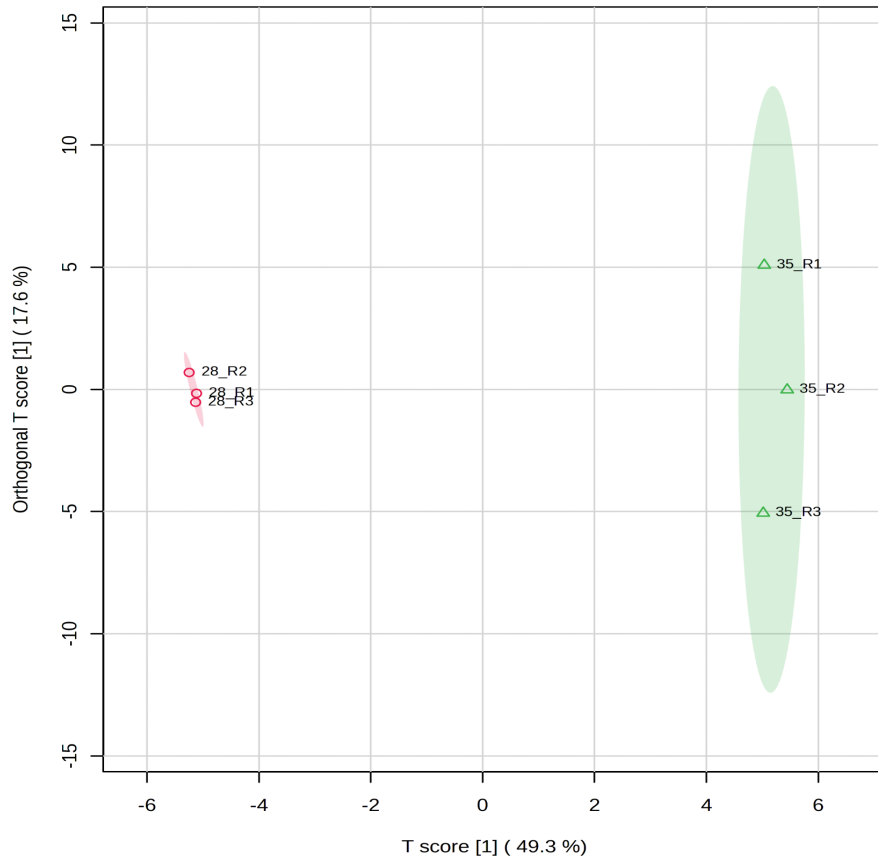


Fig 12: The OPLS-DA score plot for ICM data. Clear separation of 28°C and 35°C groups along the t[1] axis, indicates that the predictive component captures meaningful differences in the two profiles. The lack of systematic clustering of the two groups along the orthogonal t[1] axis confirms that the orthogonal variance (or noise) is irrelevant to the temperature differences and has been appropriately minimized.

OPLS-DA Model Summary:

For the OPLS-DA model, R^2Y and Q^2 are two important metrics used to assess the goodness-of-fit and predictive ability of the OPLS-DA model. Additionally, permutation tests were also performed to verify the reliability of these metrics.

	p1	o1
R2X	0.493	0.176
R2Y	0.991	0.0086
Q2	0.917	0.0246

Fig 13: Values for the OPLS-DA model for ICM. P1 and O1 represent the predictive and the orthogonal components of the data, respectively. P1 values (R^2X , R^2Y , Q^2) are desirable and should be high, as they indicate meaningful variance that explains

group differences, while O1 values (R^2X , R^2Y , Q^2) should ideally be small, as they represent orthogonal variance (noise or irrelevant variation).

For ICM data, the numbers from the figure above can be interpreted as follows:

- R^2X is the sum of predictive + orthogonal variation in X that is explained by the model, $0.176 + 0.493 = 0.669$. Can also be interpreted that 66.9% of the total variation in X is explained by the model.
- R^2Y is the total sum of variation in Y explained by the model, here $0.991 + 0.0086 = 0.9996$ or 99.96% of the variation in Y.
- Of this, 49.3% (predictive variation) of X (the metabolites) correlates directly to 99.96% of the variation in Y, while the rest of the modeled X variation (17.6%) is orthogonal and irrelevant to Y.
- Q^2 is the predictive ability of the model, i.e. how well the model generalizes to new data, which ranges from $-\infty$ to 1, and here it is 0.917.

3.4 Differentially Expressed Intracellular Metabolites

A total of 20 differential intracellular metabolites with VIP scores greater than one and $p < 0.05$ were identified as potential metabolic markers between the two groups. The levels of 9 substances were down-regulated, and the levels of 11 were upregulated.

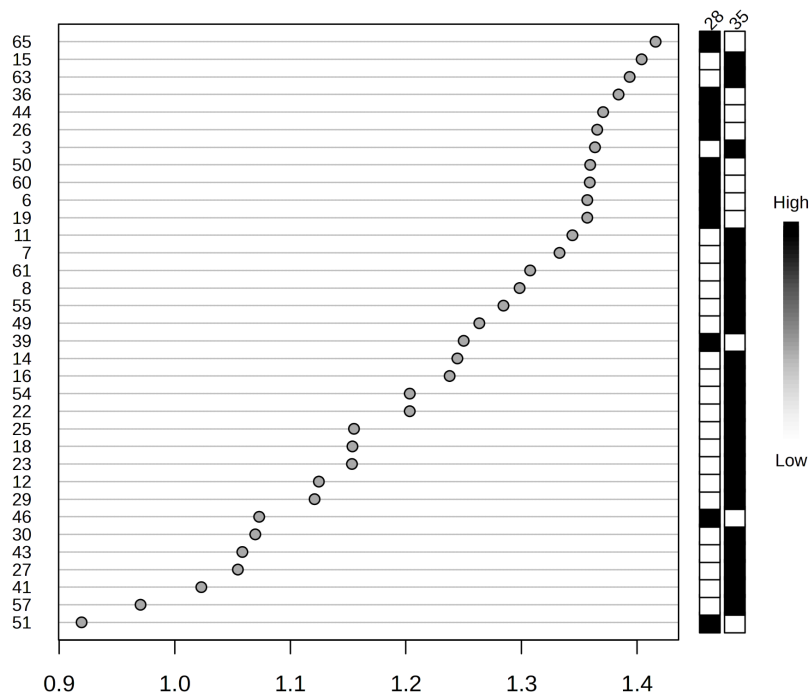


Fig 14: VIP values chart for metabolites. A total of 32 metabolites were found to have $VIP > 1$.

	Compound Name	Type	VIP Score	P-value	Regulation
1	2-Hydroxyglutaric acid	Dicarboxylic acid	1.403898244	0.00047835	Up
2	Uracil	Nucleotide	1.393560738	0.00046314	Up
3	Hydroxy-methylpent-ene naphthalene aldehyde	Aromatic	1.363547047	0.002045	Up
4	10-Heptadecenoic acid	Fatty Acid	1.344036748	0.0037272	Up
5	Dec-2-enoic acid	Fatty Acid	1.332891778	0.0055192	Up
6	5-nitrobarbiturate	Nitro Compounds	1.307482065	0.0092089	Up
7	1-Monolinolein	Mono glycerides	1.298330335	0.0096697	Up
8	Phosphoric acid	Carboxylic acid	1.284389944	0.011358	Up
9	Myo-Inositol	Sugar	1.263519978	0.018852	Up
10	Morpholine-naphthol derivative	Aromatic	1.244523415	0.025966	Up
11	2-linoleoylglycerol	Lipid	1.237826659	0.024491	Up
12	Palmitic Acid	Fatty Acid	1.20332866	0.029423	Up
13	4-Estren-4-chloro-17.beta.-ol-3-one	Steroid	1.20331034	0.033264	Up
14	Xylitol	Sugar Alcohols	1.415975974	6.49E-05	Down
15	D-Fructose	Sugar	1.383958166	0.001601	Down
16	Heptanoic acid	Fatty Acid	1.370587094	0.0026956	Down
17	8-Hexadecyne	Alkynes	1.365487991	0.0030238	Down
18	Aminomethylmethacrylamide	Aromatic	1.359401662	0.0038766	Down
19	Thiophenol	Aromatic	1.359034596	0.0041266	Down
20	Acetylhydroxy-tetramethyl naphthalene propene acid	Aromatic	1.356913056	0.0039417	Down
21	3,4,8-Trihydroxycoumarin	Aromatic	1.356890154	0.0037628	Down
22	D-Trehalose	Sugar	1.249982128	0.024266	Down

Fig 15: The list of 22 intracellular metabolites which are differentially regulated due to temperature.

Among the eleven upregulated metabolites, several belong to key metabolic classes, including dicarboxylic acids (2-Hydroxyglutaric acid), fatty acids (10-Heptadecenoic acid, Dec-2-enoic acid, Palmitic acid), aromatic compounds (Hydroxy-methylpent-ene naphthalene aldehyde, Morpholine-naphthol derivative), and sugars (Myo-Inositol, 2-linoleoylglycerol). The nine downregulated metabolites are also varied in composition, belonging to groups such as sugars (D-Fructose, D-Trehalose), fatty acids (Heptanoic acid), aromatic compounds (Aminomethylmethacrylamide, Thiophenol), and sugar alcohols (Xylitol).

Enrichment analysis further identified several key metabolic pathways being altered. The top three included Starch and Sugar metabolism, Galactose metabolism and Ascorbate and Aldarate metabolism with low p-values (< 0.05) and high enrichment ratios (= observed hits/expected hits). These were due to D-Fructose, D-Trehalose and myo-inositol being differentially regulated.

Other pathways also being altered included but with slightly higher p-values (< 0.067) included Fructose and Mannose metabolism (p-value 0.0634), Pantothenate and CoA biosynthesis (p-value 0.0634), and beta-Alanine metabolism (p-value 0.0665).

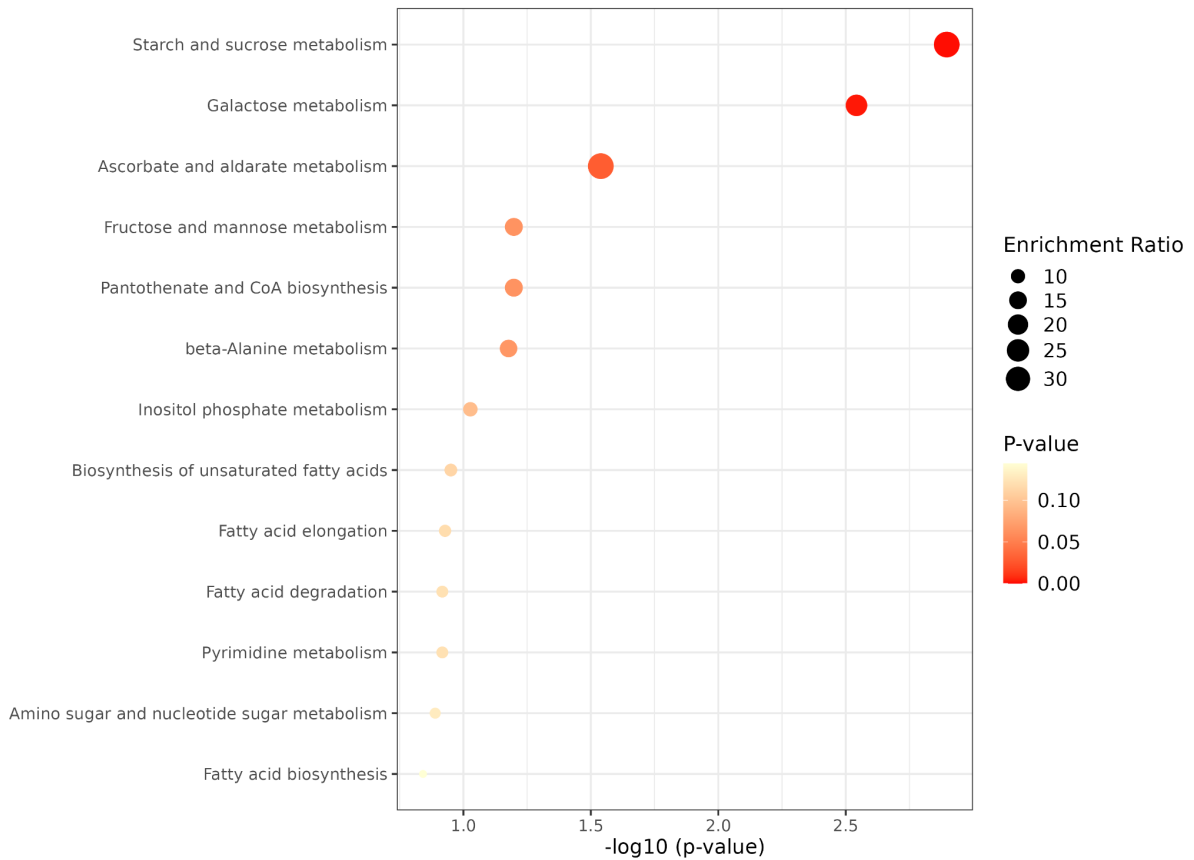


Fig 16: Overview of the enriched metabolic pathways for ICM.

4. Results for ECM

This section covers the analysis of results for extracellular metabolites. A total of 50 metabolites were submitted for analysis.

4.1 PCA Analysis

The PC1 and PC2 components explained 57.5% and 14.1% of the variance in the ECM data, respectively, together making up 71.6% of the total variance.

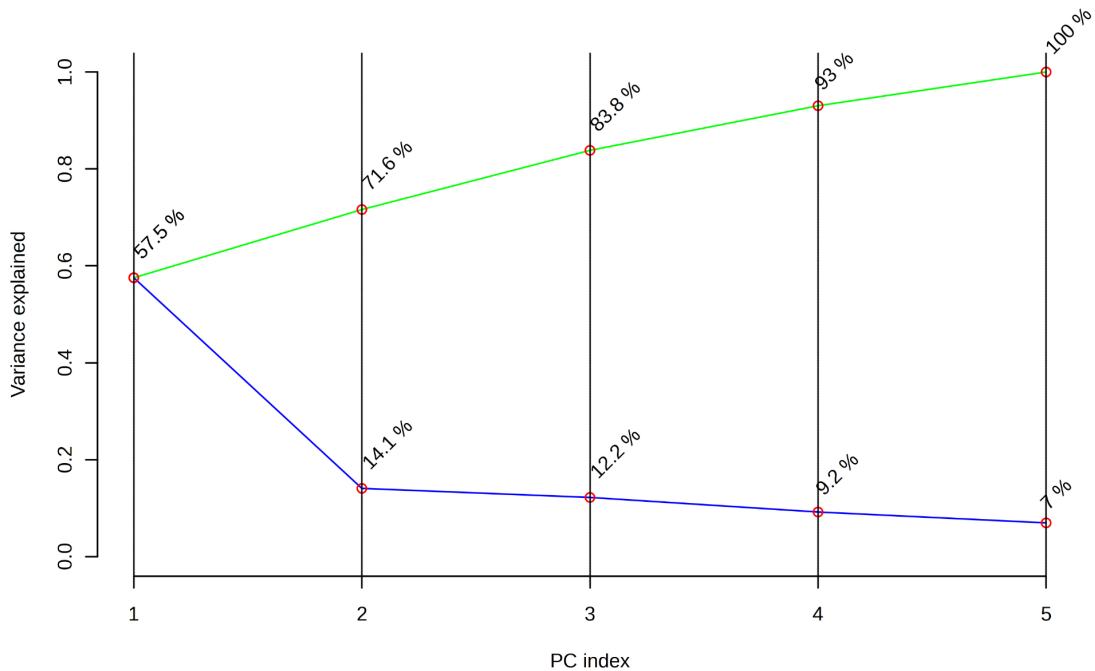


Fig 17: Scree Plot for ECM data with PC1 and PC2 accounting for a total of 71.6% of the variance.

Similar to ICM, the scores plot here also demonstrated a clear distinction between the replicates of both temperatures, with 28°C clustering on the left and 35°C on the right, all contained within the shaded 95% confidence interval. This suggests that temperature induces significant variations in extracellular metabolism as well.

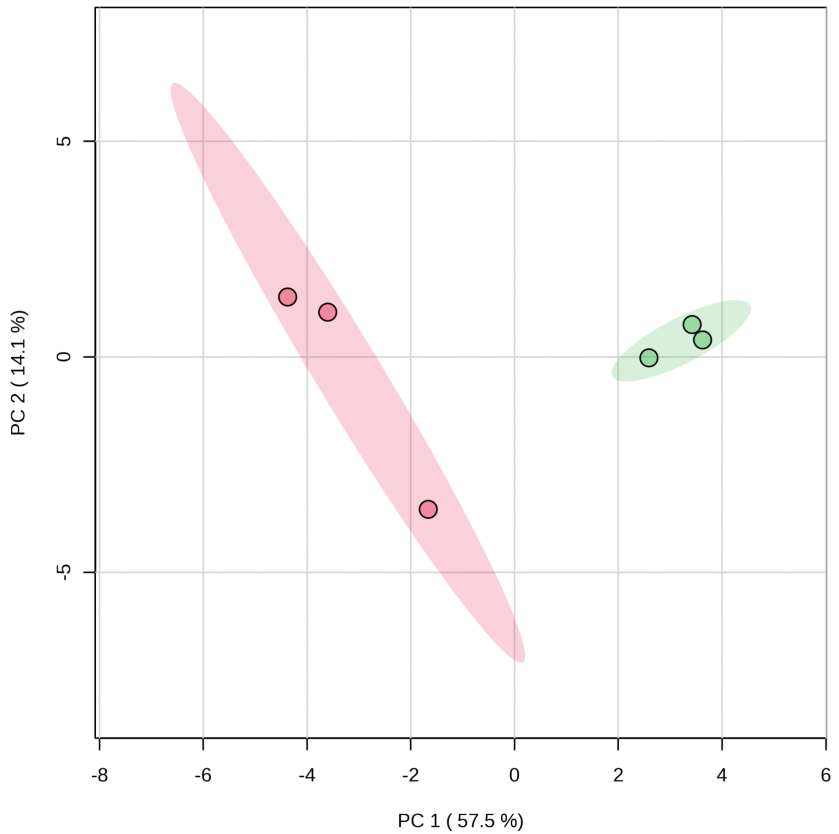


Fig 18: PCA Scores Plot for ECM data showing clear separation of both groups.

4.2 Fold Change Analysis and Volcano Plot

The FC threshold of 2 gave us 16 significantly downregulated metabolites and 19 significantly upregulated metabolites.

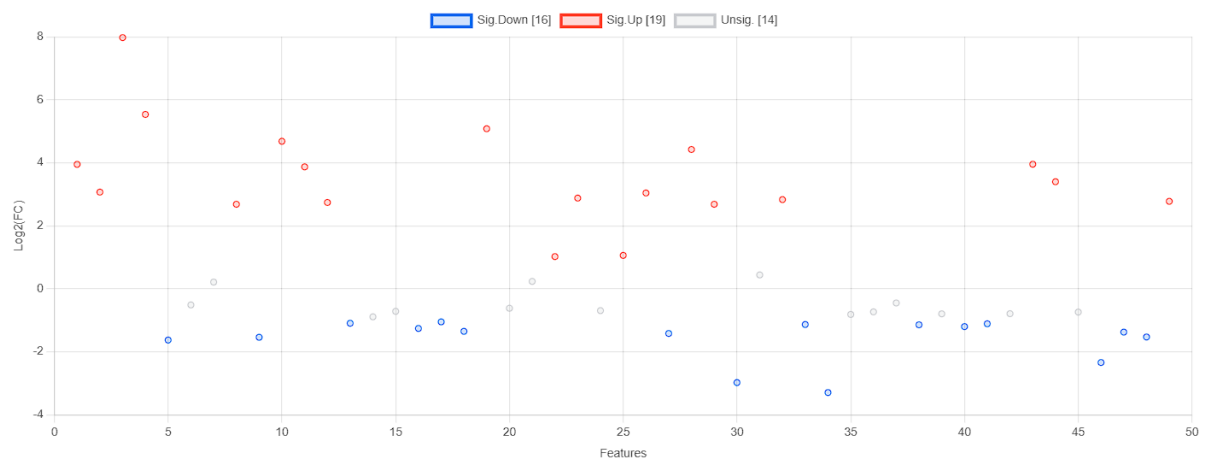


Fig 19: Fold Change (FC=2) Analysis Chart for ECM.

Upon performing a student's t-test with a significance threshold of $p < 0.05$, 15 features were identified as statistically significant, while the remaining 35 features were found to be non-significant.

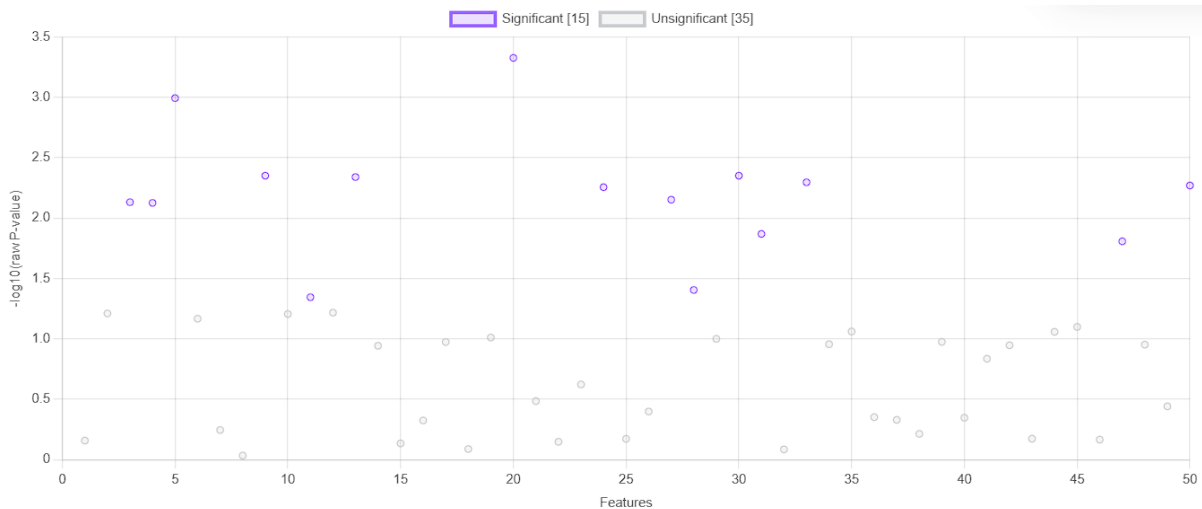


Fig 20: Student's t-test with a confidence level of 95% gives us 15 significant extracellular metabolites.

Interestingly, the volcano plot gave us only three significantly downregulated metabolites and twelve significantly upregulated metabolites.

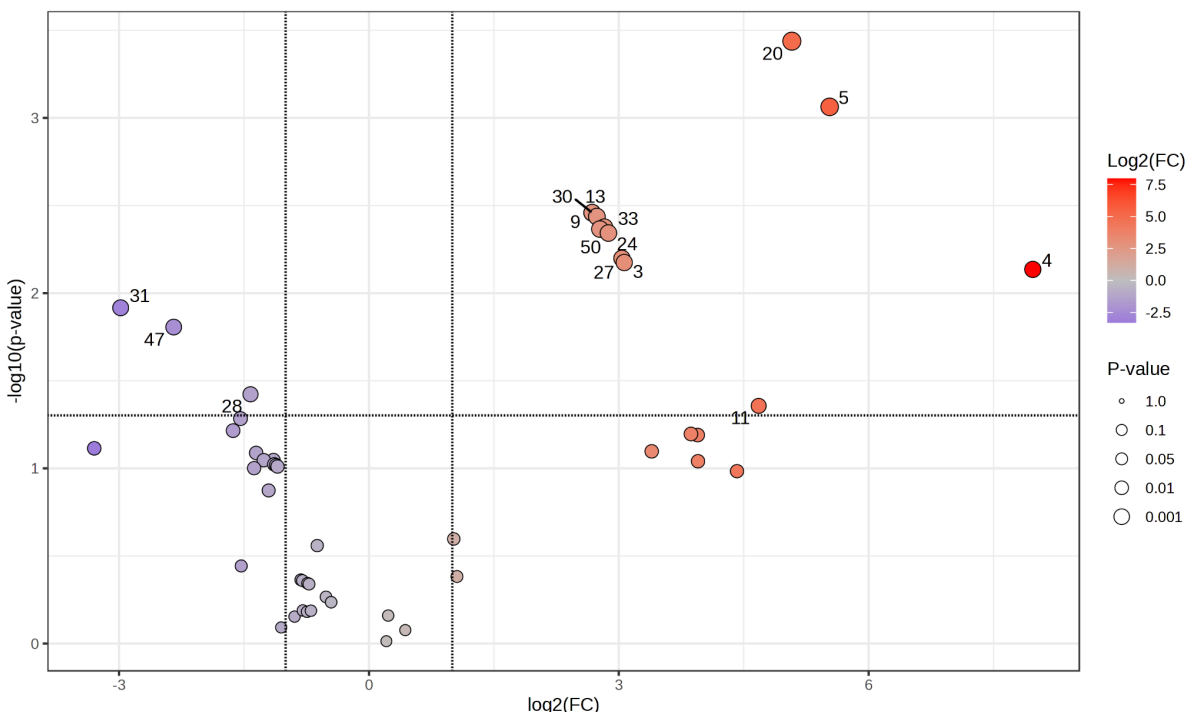


Fig 21: Volcano Plot for ECM data showcasing the three downregulated metabolites in violet and the twelve upregulated metabolites in red.

4.3 OPLS-DA

The OPLS-DA score plot for ECM data showed a clear separation of 28°C and 35°C groups along the t[1] axis, indicating that the predictive component captured meaningful differences in the two profiles. Additionally, the absence of systematic clustering of the groups along the orthogonal t[1] axis indicates that the orthogonal variance (or noise) unrelated to temperature differences was appropriately minimized.

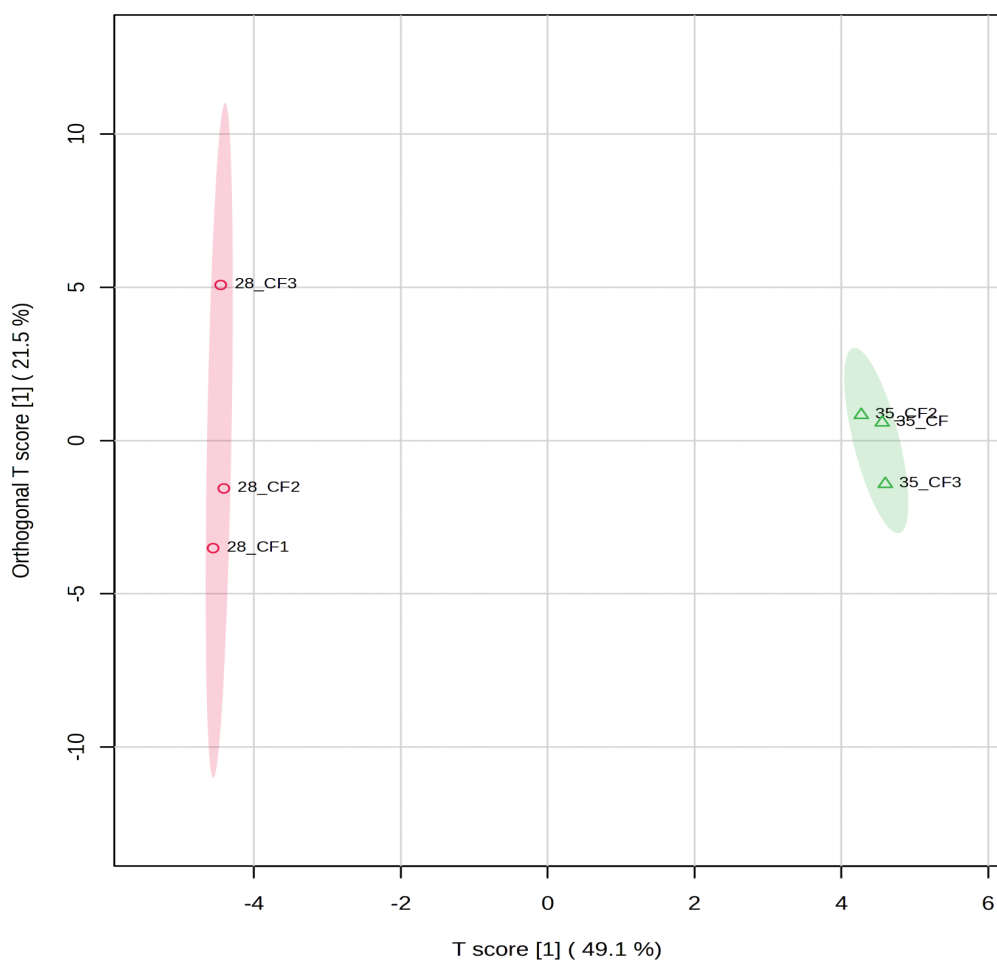


Fig 22: The OPLS-DA Score Plot for ECM data.

OPLS-DA Model Summary:

	p1	o1
R ² X	0.491	0.215
R ² Y	0.93	0.0692
Q ²	0.838	0.0671

Fig 23: The reliability metrics for the OPLS-DA model for ECM. With the metrics being similar to ICM, we could confirm that the model was working well.

For ECM data, the numbers from the figure above can be interpreted as follows:

- R²X represents the total variation in X explained by the model, with 70.6% explained (0.215 + 0.491).
- R²Y shows the total variation in Y explained, with 99.92% explained (0.93 + 0.0692).
- Of this, 49.1% of X (metabolites) correlates to 99.92% of Y, while 21.5% is orthogonal (irrelevant to Y).
- Q², the model's predictive ability, is 0.838, indicating strong generalization to new data.

4.4 Differentially Expressed Extracellular Metabolites

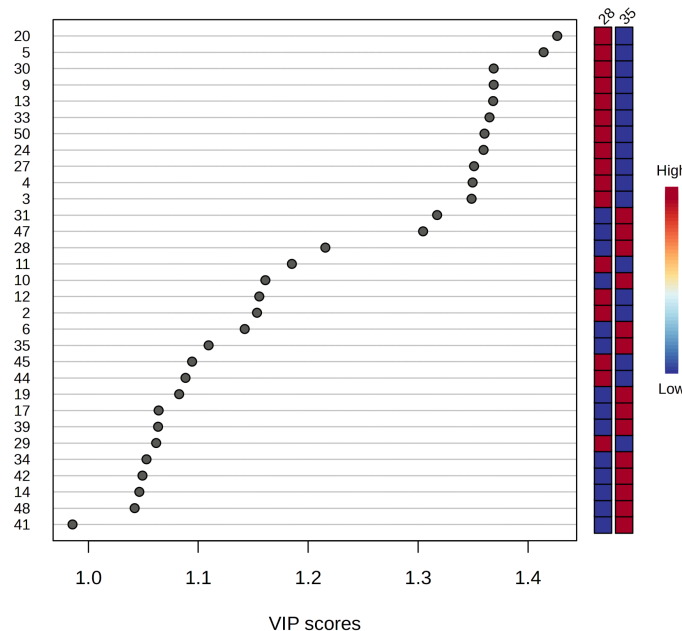


Fig 24: VIP values chart for metabolites. A total of 30 metabolites were found to have $VIP > 1$.

A total of 15 differential extracellular metabolites with VIP scores greater than one and $p < 0.05$ were identified. The levels of 12 substances were down-regulated, and the levels of 3 were upregulated.

	Compound Name	Type	P-value	VIP Score	Regulation
1	Glycerol	Sugar Alcohol	0.013532	1.317336695	Up
2	Serine	Amino Acid	0.015573	1.304557349	Up
3	DL-Phenylalanine	Amino Acid	0.039401	1.21563116	Up
4	D-Arabinose	Monosaccharide	0.00047159	1.426624576	Down
5	1-Phenyl-1,2-ethanediol	Aromatic Alcohol	0.0010163	1.414247467	Down
6	2-Isopropyl butyric acid	Fatty Acid	0.0044563	1.368812071	Down
7	Glyceric acid	Hydroxy Acid	0.0044563	1.368812152	Down
8	5-Hydroxymethyl-2-furoic acid	Aromatic Acid	0.0045759	1.368309928	Down
9	L-(+)-Threose	Monosaccharide	0.0050518	1.364990054	Down
10	Xylitol	Sugar Alcohol	0.0053726	1.360447342	Down
11	D-Glucitol	Sugar Alcohol	0.0055508	1.35959319	Down
12	Diethanolamine	Amine	0.007047	1.350925474	Down
13	beta-Gentiobiose	Disaccharide	0.0073855	1.348680227	Down
14	1-Deoxypentitol	Sugar Alcohol	0.0074892	1.349628766	Down
15	3,4,8-Trihydroxycoumarin	Aromatic	0.045221	1.185151802	Down

Fig 25: The list of 15 extracellular metabolites which are differentially regulated due to temperature.

Among the upregulated metabolites, Glycerol, Serine, and Phenylalanine are highlighted with relatively low p-values (< 0.04) and VIP scores above 1.2, suggesting them to be important extracellular metabolic markers distinguishing the two temperature groups. These compounds are also involved in key biochemical pathways, with Glycerol being a sugar alcohol linked to energy metabolism, and amino acids like Serine and Phenylalanine playing roles in protein synthesis and signaling.

Conversely, a much larger set of metabolites showed downregulation, belonging to categories such as monosaccharides (e.g., Arabinose and Threose), sugar alcohols (e.g., Xylitol, D-Glucitol, and 1-Deoxypentitol), and fatty acids (e.g., 2-Isopropyl butyric acid). The downregulation of sugars and sugar alcohols may point to reduced carbohydrate metabolism due to heat stress, while the decline in aromatic compounds (e.g., 3,4,8-Trihydroxycoumarin and 5-Hydroxymethyl-2-furoic acid) may indicate shifts in secondary metabolite pathways.

Interestingly, Xylitol and 3,4,8-Trihydroxycoumarin appear in both ICM and ECM datasets, with similar downregulation patterns for the 35°C group, with high VIP scores (all with $VIP > 1.1$) and low p-values, suggesting their strong potential to be metabolic markers. Studying these markers further can provide valuable insights into

the mechanisms driving the observed metabolic shifts between the two temperatures.

Enrichment analysis showed Glycerolipid metabolism, Galactose metabolism, Glyoxylate and dicarboxylate metabolism, Glycine, serine and threonine metabolism and D-Amino acid metabolism to be significantly ($p\text{-value} < 0.05$) altered between the two groups, due to the differential regulation of Glycerol, Glyceric acid, Sorbitol, and Serine.

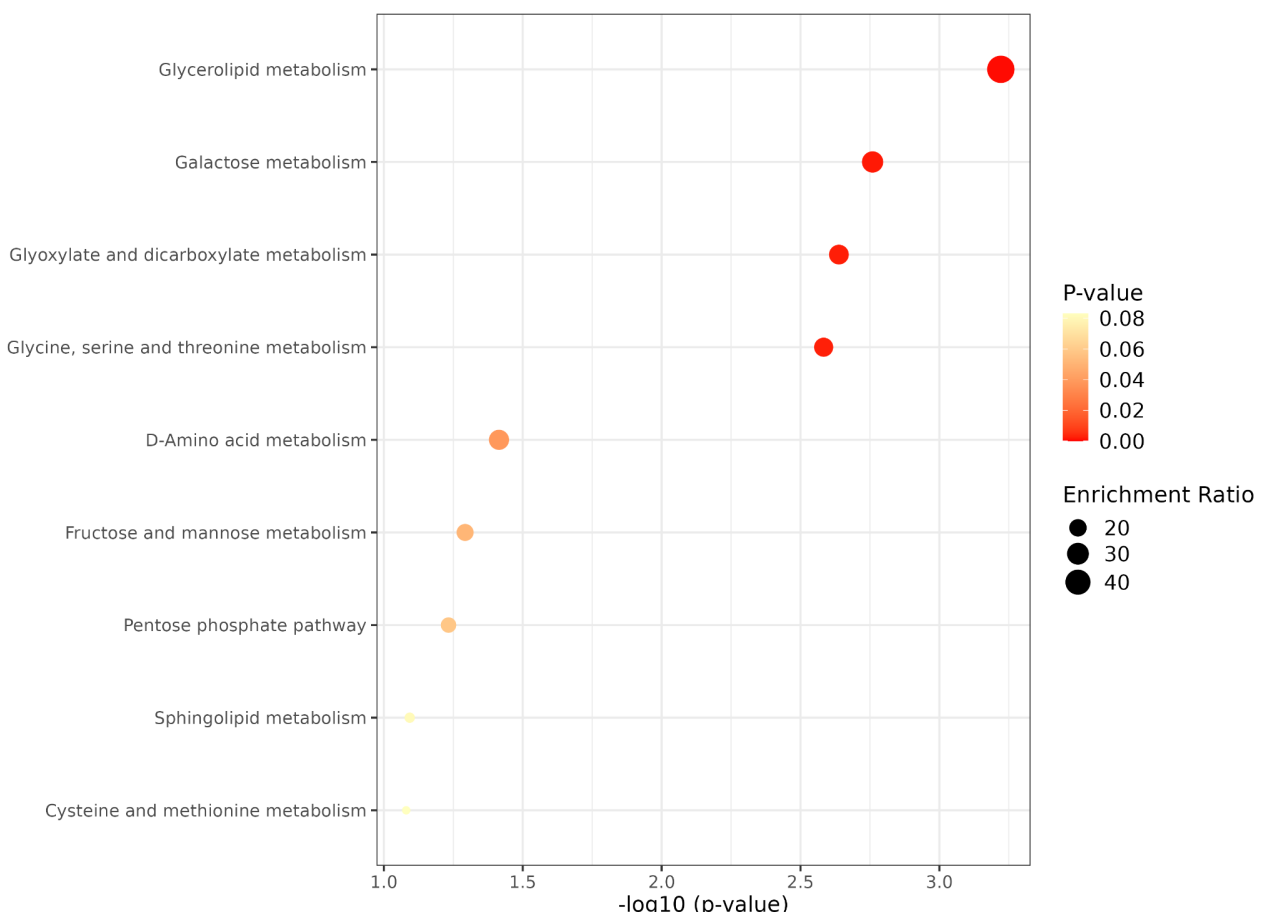


Fig 26: Overview of the enriched metabolic pathways for ECM.

5. Conclusion

This study provides a comprehensive analysis of the metabolomic shifts in *Macrophomina phaseolina* at two temperatures (28°C and 35°C), shedding light on how temperature influences both intracellular and extracellular metabolic processes. Our results demonstrate that temperature has a significant impact on the metabolic profiles of *Mp*, with distinct changes observed in both intracellular and extracellular metabolites between the two temperature conditions.

Through PCA, fold-change analysis, and OPLS-DA, we identified several differential metabolites, some of which can be potential metabolic markers that could be targeted for future studies or interventions to mitigate *Mp*-induced root rot. Notably, two distinct metabolites, Xylitol, and 3,4,8-Trihydroxycoumarin, appeared to be downregulated in both intracellular and extracellular datasets.

In conclusion, this study highlights the significant impact of temperature on the metabolic landscape of *Macrophomina phaseolina*. The insights gained from this research could guide the development of strategies for crop protection, such as identifying novel targets for resistant crop breeding or the design of antifungal treatments, ultimately helping to mitigate the future risks posed by this pathogen under climate change scenarios.

6. References for Chapter 3

1. Khambhati, V. H., Abbas, H. K., Sulyok, M., Tomaso-Peterson, M., Chen, J., & Shier, W. T. (2023). Mellein: Production in culture by *Macrophomina phaseolina* isolates from soybean plants exhibiting symptoms of charcoal rot and its role in pathology. *Frontiers in Plant Science*, 14. <https://doi.org/10.3389/fpls.2023.1105590>
2. Basandrai, A. K., Pandey, A. K., Prakit Somta, & Basandrai, D. (2021). *Macrophomina phaseolina*–host interface: Insights into an emerging dry root rot pathogen of mungbean and urdbean, and its mitigation strategies. *Plant Pathology*, 70(6), 1263–1275. <https://doi.org/10.1111/ppa.13378>
3. Alam, S., Abbas, H. K., Sulyok, M., Khambhati, V. H., Okunowo, W. O., & Shier, W. T. (2022). Pigment Produced by Glycine-Stimulated *Macrophomina Phaseolina* Is a (−)-Botryodiplodia Reaction Product and the Basis for an In-Culture Assay for (−)-Botryodiplodia Production. *Pathogens*, 11(3), 280–280. <https://doi.org/10.3390/pathogens11030280>
4. Almudena García-García, Cuesta-Valero, F. J., Miralles, D. G., Mahecha, M. D., Quaas, J., Reichstein, M., Jakob Zscheischler, & Peng, J. (2023). Soil heat extremes can outpace air temperature extremes. *Nature Climate Change*, 13(11), 1237–1241. <https://doi.org/10.1038/s41558-023-01812-3>

Chapter 4: The Cell Wall

“Characterization of *Macrophomina phaseolina* Cell Wall: Insights into Pathogenicity and Plant Immunity Interactions”

1. Introduction

In this study, we profiled the cell wall (CW) of *Macrophomina phaseolina* grown at 28°C, a temperature optimal for its growth. To achieve this, CW material was isolated as alcohol insoluble residues (AIR), which were further fractionated using alkali treatments.

The alditol acetate method was used to determine the monosaccharide composition of the fractions, while permethylated alditol acetates were used to identify the key glycosidic linkages. The results of these two methods showed that there are significant differences in the monosaccharide composition and glycosidic binding profiles among the CW fractions.

These compositional variations suggested that the CW fractions may evoke differential plant immunogenicity, potentially influencing plant defense responses. To investigate this hypothesis, we evaluated the immune activity of the CW fractions in Soybean leaf systems using early pattern-triggered immunity (PTI) markers, specifically measuring transient reactive oxygen species (ROS) bursts.

2. Materials and Methods

2.1 Isolation of Alcohol Insoluble Residue (AIR)

Freeze-dried mycelium was added to a sterile mortar, to which 40 mL of 70% ethanol was added and ground until homogenized. The mixture was centrifuged at 14,000 RPM for 10 minutes at RT. The supernatant was discarded, and 40 mL of chloroform:methanol (1:1) was added to delipidify the pellet. After vortexing thoroughly, it was centrifuged at 14,000 RPM for 10 minutes at RT, and the supernatant was discarded. 500 μ L of 100% acetone was added to the pellet and dried under a fume hood for 4 hours. After purging a few times with nitrogen gas, it was kept in a vacuum desiccator until the resultant AIR sample was completely dried.

2.2 Preparation of Alkali-insoluble (AKI) and Alkali-Soluble (AKS)

To prepare the AKI and AKS fractions, 0.5 g of AIR was weighed into 50 mL falcon tubes, to which 20 mL of alkali solution (1 M NaOH and 10 mM NaBH₄) was added. The mixture was gently vortexed and incubated at 75°C for 2 hours. Following incubation, the tubes were centrifuged at 12,000 RPM at RT to separate the supernatant (AKS) from the pellet (AKI).

2.3 Processing of the AKS Fraction

The supernatant (AKS) was divided into two separate tubes, each containing 10 mL. To precipitate the AKS/I fraction, pre-cooled glacial acetic acid was added to each tube in an equal volume, and checked with pH strips to ensure an acidic environment. Subsequently, 30 mL of ice-cold 100% ethanol was added, and the mixture was incubated at -20°C overnight. The precipitated AKS/I fraction was then recovered by centrifuging at 12,000 RPM for 15 minutes, and the resulting pellet was washed with 70% ethanol, followed by dialysis to remove impurities, and lyophilized for storage.

AIR	AKS/I	% Yield
5 g	300 mg	6%

Fig 27: Yield table recording of AKS/I obtained from AIR. To maximize AKS/I output, only 0.5 g of AIR was treated at a time.

2.4 Processing of the AKI Fraction

The AKI pellet was washed thoroughly with 70% ethanol to remove residual impurities. After washing, the pellet underwent dialysis to ensure purity, followed by lyophilization to obtain a dry, storable AKI fraction.

2.5 Monosaccharide Analysis

Studying the monosaccharide composition broadly included alditol acetate derivatization, reduction, and acetylation, followed by clean-up and GC-MS analysis as described by Liu et al. (2021). Trifluoroacetic acid (TFA) hydrolysis was performed on 5 mg of each sample (AIR, AKI, AKSI), to which 300 µL 2M TFA was added. The sample was heated at 121°C for 90 minutes, after which the TFA was evaporated under a stream of nitrogen gas at 45°C. This was then reduced with 10 mg/mL of sodium borodeuteride (NaBD_4) in 1 M of NH_4OH and incubated at RT for 60 minutes. The solution was neutralized with 150 µL of glacial acetic acid. This was followed by the addition of 300 µL methanol:acetic acid (9:1, v/v). The mixture was evaporated, followed by 3 washes with 300 µL methanol. Acetylation was performed by adding 50 µL acetic anhydride and 50 µL pyridine, and the mixture was incubated at 121°C for 30 minutes, followed by two washes with 200 µL toluene. The sample was cleaned up by dissolving in ethyl acetate and water, where the alditol acetates dissolved in the organic phase. The ethyl acetate was evaporated, and acetone was added to dissolve the derivatized sugars. Finally, 100 µL was transferred to GC-MS vials for analysis. The obtained spectrum was identified through retention time and the mass spectrum of standard sugars.

2.6 Glycosidic Linkage Analysis

Linkage analysis was done as described in Sen-Itiroh Hakomori et al. (1964). To put it briefly, 4 mg per sample was taken (AIR, AKI, AKSI) to which dry DMSO was added. The tubes were sonicated and kept for stirring at RT overnight. Prepared NaOH/DMSO was added and methylation was carried out by adding methyl iodide and purged with nitrogen gas, and kept for stirring gently for 2.5 hours. The samples were bubbled with nitrogen and dichloromethane was added. After the organic solvent was dried, these samples were subjected to hydrolysis and alditol acetate derivatization similar to the method utilized in monosaccharide analysis to obtain partially methylated alditol acetates (PMAs). The linkages were then manually identified based on their retention times and through their mass spectrum fragmentation patterns through comparison with the CCRC Spectral Database for PMAs.

2.7 Quantification Assays

For the phenol sulphuric acid assay, anthrone assay and the biphenyl assay, TFA hydrolysis was first conducted similar to monosaccharide and linkage analysis in order to facilitate the hydrolysis of glycosidic bonds and release sugars from their complex polymers. To each sample, 300 µL 2M TFA was added and heated for 90 minutes at 121°C. The tubes were cooled on ice and the supernatant was collected after centrifugation, which was then used for the assays.

2.7.1 General Sugars and Hexoses

For estimating the quantity of total sugars, we performed a simple and reliable colorimetric assay, the phenol sulphuric acid assay (DuBois et al., 1956). This involved transferring 100 µL of sample fraction to a Pyrex glass tube, to which 100 µL H₂O was added, followed by 200 µL 5% phenol (5.5 ml 90% phenol dissolved in 94.5 mL H₂O). The tube was then vortexed thoroughly, and 1 mL conc. H₂SO₄ was added rapidly and carefully. Following this, the tubes were cooled off for 20 minutes at RT, and then 200 µL was transferred to a 96-well microtiter plate and absorbance was taken at 490 nm.

Hexoses (glucose, fructose, galactose, etc.) were estimated using the anthrone assay (Graham & J. Smydzuk, 1965). Again, 100 µL of sample fraction was transferred to a Pyrex glass tube, to which 150 µL H₂O was added, followed by 500 µL of 0.2% (w/w) anthrone reagent (1 g anthrone in 500 mL conc. H₂SO₄). After vortexing thoroughly, the tube was heated for 5 minutes at 100°C and then cooled for 10 minutes at RT. After this, 200 µL was transferred to a 96-well microtiter plate, and absorbance was taken at 620 nm.

For both assays, a standard curve of varying glucose concentrations was used to extrapolate the samples.

2.7.2 Uronic acids

The biphenyl assay (Filisetti-Cozzi & Carpita, 1991) was performed to estimate uronic acids in the fractions, which employed two reagents: 12.5 mM sodium borate buffer (4.77 g NaB₄O₇.10H₂O in 1 L H₂SO₄) and 0.15% m-hydroxy-biphenyl in 0.5% NaOH.

To perform the assay, 100 µL of the sample was transferred to a Pyrex glass tube, to which 600 µL of the sodium borate buffer was added. The tubes were vortexed thoroughly, then heated for 5 minutes at 100°C. After cooling the tubes for 10 minutes at RT, 10 µL biphenyl solution was added, and 200 µL was transferred to a microtiter plate. Absorbance was taken at 520 nm after a 10 minute wait. This assay employed varying concentrations of D-glucuronic acid (15.625 µg/mL to 500 µg/mL) as a standard.

2.7.3 Chitin estimation

For chitin estimation, a colorimetric assay using a silica-molybdate (Si(IV)-Mo(VI)) reagent was employed (Hajime Katano et al., 2016). To prepare this, 0.1 M Na₂SiO₃ and 1.2 M Na₂MoO₄ were added to 50 mL MQ, followed by stirring for 2 hours.

A reagent mix was then prepared by combining 5 mL of the Si(IV)-Mo(VI) solution, 3 mL DMSO, and 1.5 mL 10 M acetic acid. The final volume of the reagent mix was made up to 10 mL, which achieved a composition of 50 mM Na₂SiO₃, 600 mM Na₂MoO₄, 1.5 M CH₃COOH, and 30% (v/v) DMSO. The solution was placed on a rocker for 2–4 hours to ensure complete homogenization.

To prepare the *Mp* fractions for chitin analysis, 10 mg of each sample was hydrolyzed in 10 mL of 5 M HCl at 100°C for 12 hours to release glucosamine from their complex polymeric forms. The hydrolysate (20 µL) was neutralized with 20 µL of 5 M NaOH, followed by the addition of 200 µL of the reagent mix. The reaction was incubated at 70°C for 30 minutes, and the absorbance at 750 nm was recorded. Chitin content for the fractions was calculated by extrapolating against a glucosamine standard curve (200 µg/mL to 1 mg/mL).

2.8 ROS Burst Assay

ROS Burst Assay for the Soybean leaf system was performed according to Muthusaravanan et al. (2023). Leaves were selected from day 10 Soybean plants in the trifoliate stage.

3. Results

3.1 Monosaccharide Analysis

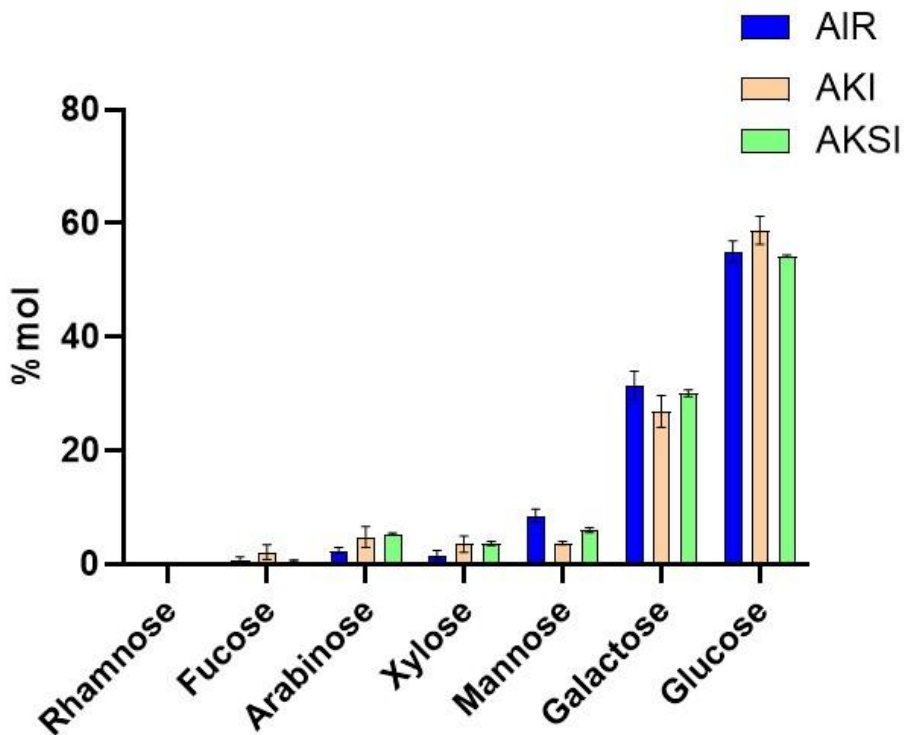


Fig 28: Monosaccharide estimation (%mol) in the different fractions

	AIR vs. AKI		AIR vs. AKSI		AKI vs. AKSI	
	P-value	Significant	P-value	Significant	P-value	Significant
Rhamnose	0.9998	No	0.9931	No	0.995	No
Fucose	0.3727	No	0.9891	No	0.3025	No
Arabinose	0.0756	No	0.022	Yes*	0.8574	No
Xylose	0.1614	No	0.1273	No	0.9915	No
Mannose	<0.0001	Yes****	0.045	Yes*	0.089	No
Galactose	0.0002	Yes***	0.4054	No	0.0095	Yes**
Glucose	0.0024	Yes**	0.7429	No	0.0003	Yes***

Fig 29: Monosaccharide analysis comparison between the fractions, the significantly altered compositions have been highlighted in green.

Where, one star (*) = p-value less than 0.05, two stars (**) = p-value less than 0.01, three stars (***) = p-value less than 0.001, and four stars (****) = p-value is less than 0.0001.

3.2 Glycosidic Linkage Analysis

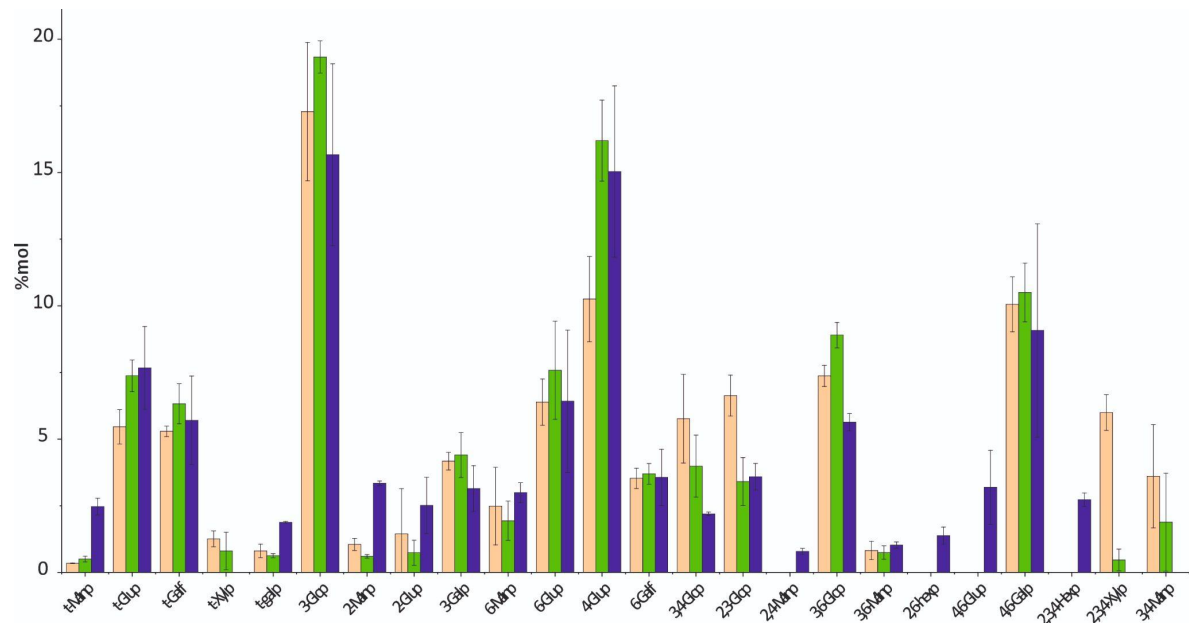


Fig 30: Glycosidic linkage estimation (%mol) in the different fractions (AKI is orange, AKSI is green, while AIR is purple).

No.	Linkage	AIR vs. AKI		AIR vs. AKSI		AKI vs. AKSI	
		P-value	Significant	P-value	Significant	P-value	Significant
1	t-Manp	0.0673	No	0.0989	No	0.984	No
2	t-Glup	0.055	No	0.9482	No	0.1115	No
3	t-Galf	0.9022	No	0.7886	No	0.5222	No
4	t-Xylp	0.3832	No	0.6749	No	0.8811	No
5	t-Galp	0.4958	No	0.3858	No	0.9805	No
6	3-GlcP	0.2069	No	0.0005	Yes***	0.0817	No
7	2-Manp	0.0445	Yes*	0.0124	Yes*	0.8849	No
8	2-Glup	0.4967	No	0.1498	No	0.738	No
9	3-Galp	0.5263	No	0.3823	No	0.9675	No
10	6-Manp	0.8532	No	0.5057	No	0.8316	No
11	6-Glup	0.9992	No	0.4418	No	0.4201	No
12	4-Glup	<0.0001	Yes****	0.4435	No	<0.0001	Yes****
13	6-Galf	0.9993	No	0.9893	No	0.983	No
14	3,4-GlcP	0.0007	Yes***	0.1465	No	0.1486	No
15	2,3-GlcP	0.0046	Yes**	0.9802	Yes**	0.0025	No
16	2,4-Manp	0.6865	No	0.6865	No	>0.9999	No
17	3,6-GlcP	0.1642	No	0.0022	Yes**	0.2426	No
18	3,6-Manp	0.9751	No	0.9529	No	0.9963	No
19	2,6-Hexp	0.3165	No	0.3165	No	>0.9999	No
20	4,6-Glup	0.0028	Yes**	0.0028	Yes**	>0.9999	No
21	4,6-Galp	0.5582	No	0.2925	No	0.8849	No
22	2,3,4-Hexp	0.0129	Yes*	0.0129	Yes*	>0.9999	No
23	2,3,4-Xylp	<0.0001	Yes****	0.8755	No	<0.0001	Yes****
24	3,4-Manp	0.0006	Yes***	0.1191	No	0.1675	No

Fig 31: Glycosidic linkage comparison between the fractions, the significantly altered linkages have been highlighted in green.

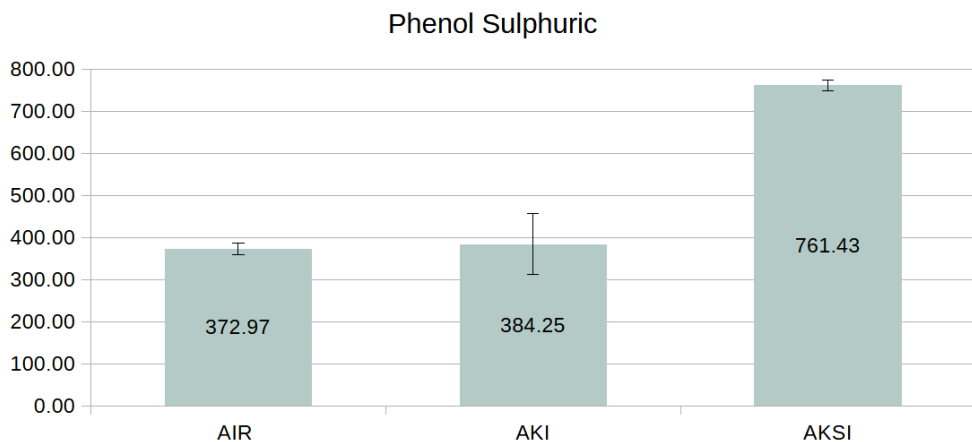
Where, one star (*) = *p*-value less than 0.05, two stars (**) = *p*-value less than 0.01, three stars (***) = *p*-value less than 0.001, and four stars (****) = *p*-value is less than 0.0001.

3.3 Quantification Assays

3.3.1 General Sugars and Hexoses

Both general sugars and hexoses were found to be the highest in the AKS/I fraction, with 761.43 µg and 642.42 µg, respectively, in one mg of sample. For AIR and AKI fractions, the amount of total sugars and hexoses were comparable, with AKI leading in total sugars by 11.28 µg/mg and AIR leading in hexoses by 13.04 µg/mg.

a)



b)

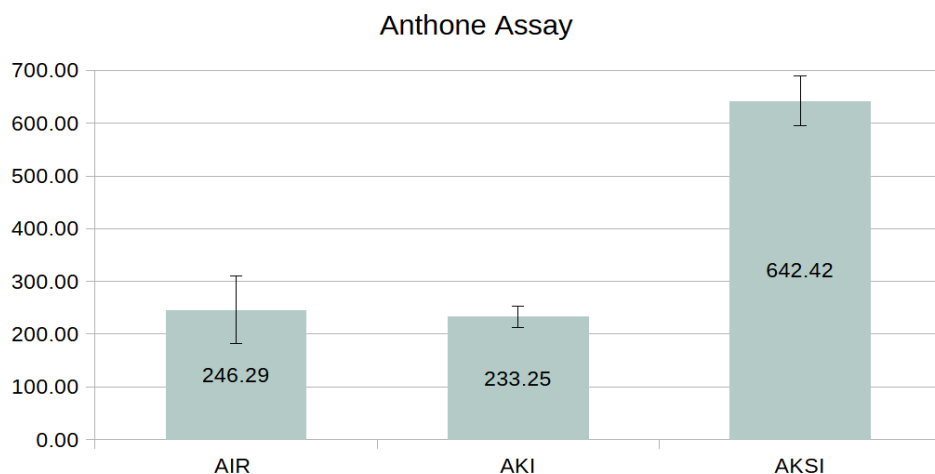


Fig 32: Estimation of a) total sugars, and b) hexoses in the different fractions.

3.3.2 Uronic acids

AKS/I fraction had the highest quantity of uronic acids as well (188.55 µg/mg) followed by comparable quantities in AIR and AKI, with AKI having the lowest quantity by 13.94 µg/mg.

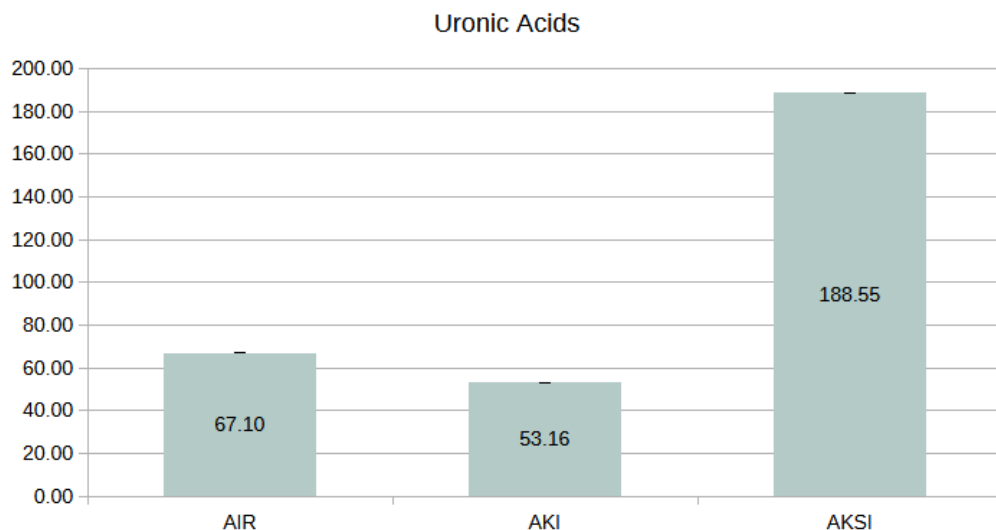


Fig 33: Estimation of uronic acids in the different fractions.

3.3.3 Chitin estimation

Chitin estimation of the three fractions showed AKS/I to have the highest quantity with 137 µg/mg, followed by AKI with 110.65 µg/mg and then AIR with 97.87 µg/mg.

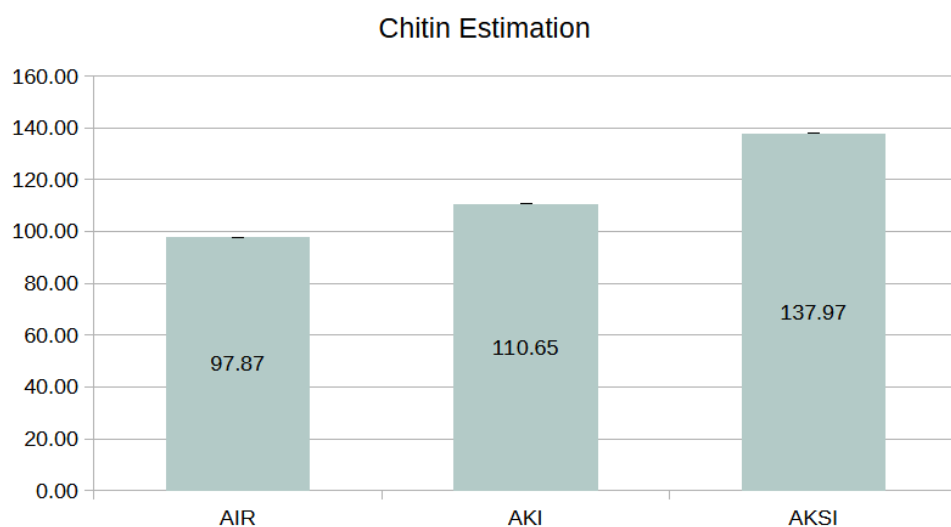


Fig 34: Estimation of chitin in the different fractions.

3.4 ROS Burst Assay

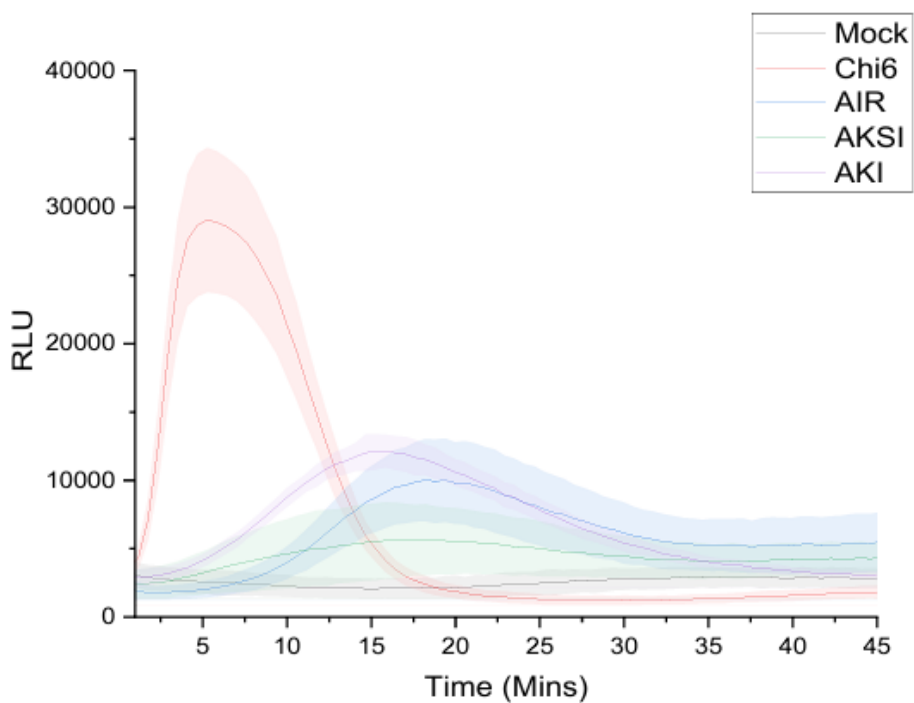


Fig 35: Graph showing ROS burst for the different fractions. AKI shows the highest burst, followed by AIR and then AKSI.

4. Conclusion

This study provides a comprehensive characterization of the cell wall (CW) of *Macrophomina phaseolina*, offering insights into its biochemical composition, and its potential interactions with plant immunity. The isolation and fractionation of CW material into alkali-soluble (AKS) and alkali-insoluble (AKI) fractions, along with detailed monosaccharide and glycosidic linkage analyses, revealed significant differences in composition between these fractions. Notably, the AKS/I fraction displayed the highest abundance of general sugars, hexoses, uronic acids, and chitin, highlighting its polysaccharide-rich nature.

The ROS burst assay indicated that the AKI fraction triggered the strongest early plant immune response, followed by AIR and AKS/I. This suggests that the structural and compositional differences in CW fractions influence their immunogenicity, potentially affecting their interaction with plant defense mechanisms.

The findings underline the complexity of the fungal CW as a multifaceted structure. By linking CW composition to plant immune activity, this study contributes to a deeper understanding of the pathogenic strategies of *Mp* and highlights potential targets for developing effective plant protection strategies.

In future studies, the immune activity of the CW fractions in root and leaf systems could be validated further by investigating late pattern-triggered immunity (PTI) markers, such as callose deposition and cytotoxicity assays. Moreover, the potential of the CW fractions to act as priming agents can be explored further by infection assays through developing elicitor formulations.

5. References for Chapter 4

1. DuBois, M., Gilles, K. A., Hamilton, J. K., Rebers, P. A., & Smith, F. (1956). Colorimetric Method for Determination of Sugars and Related Substances. *Analytical Chemistry*, 28(3), 350–356. <https://doi.org/10.1021/ac60111a017>
2. Liu, D., Tang, W., Yin, J.-Y., Nie, S.-P., & Xie, M.-Y. (2021). Monosaccharide composition analysis of polysaccharides from natural sources: Hydrolysis condition and detection method development. *Food Hydrocolloids*, 116, 106641–106641. <https://doi.org/10.1016/j.foodhyd.2021.106641>
3. SEN-ITIROH HAKOMORI. (1964). A Rapid Permetylation of Glycolipid, and Polysaccharide Catalyzed by Methylsulfinyl Carbanion in Dimethyl Sulfoxide. *The Journal of Biochemistry*, 55(2), 205–208. https://www.jstage.jst.go.jp/article/biochemistry1922/55/2/55_2_205/_article/-char/ja/

4. Graham, D., & J. Smydzuk. (1965). Use of anthrone in the quantitative determination of hexose phosphates. *Analytical Biochemistry*, 11(2), 246–255. [https://doi.org/10.1016/0003-2697\(65\)90012-6](https://doi.org/10.1016/0003-2697(65)90012-6)
5. Filisetti-Cozzi, T. M. C. C., & Carpita, N. C. (1991). Measurement of uronic acids without interference from neutral sugars. *Analytical Biochemistry*, 197(1), 157–162. [https://doi.org/10.1016/0003-2697\(91\)90372-z](https://doi.org/10.1016/0003-2697(91)90372-z)
6. Hajime Katano, Masahiro Takakuwa, Hayakawa, H., & Kimoto, H. (2016). Determination of Chitin Based on the Colorimetric Assay of Glucosamine in Acidic Hydrolysate. *Analytical Sciences*, 32(6), 701–703. <https://doi.org/10.2116/analsci.32.701>
7. Muthusaravanan Sivaramakrishnan, Goel, S., Nikhil Ratnaparkhi, & Chandrasekar, B. (2023). Chemiluminescence-Based Assay to Monitor Early Oxidative Bursts in Soybean (*Glycine max*) Lateral Roots. *Current Protocols*, 3(8). <https://doi.org/10.1002/cpz1.869>

Conclusion

This research advances our understanding of *Macrophomina phaseolina*, addressing its metabolic adaptations and cell wall composition as pivotal factors in its pathogenicity and host interactions.

The metabolomic analysis uncovers key biomarkers linked to heat stress and increased virulence, highlighting the impact of temperature on the pathogen's intracellular and extracellular metabolic landscape. The cell wall characterization reveals significant structural components that influence plant immune responses, establishing their potential as elicitor formulations to boost plant immunity. Together, these insights pave the way for innovative strategies to mitigate Mp-induced crop losses, particularly in the context of rising global temperatures and shifting agricultural conditions.

This study thus lays the groundwork for mitigating the impact of this fungal pathogen and ultimately developing resilient crop varieties.

Appendix A – EPS

During my thesis, I also worked on isolating extracellular polymeric substances (EPS) from residual *Mp* culture filtrate. I would like to put the process for the same below for reference, which broadly included cryogelation, deproteinization, dialysis, and lyophilization for the recovery of high-quality EPS for downstream analyses.

Isolation Process

The isolation began after *Mp* mycelia was filtered out of the culture media using a Mira cloth. The culture media was then kept at -80°C for 24 hours for cryogelation. The next day, after thawing, the precipitated EPS was collected using a pipette controller and pelleted by centrifugation at 12,000 RPM at RT for 15 minutes. The supernatant, containing the culture media was drained, and the pellet was washed thrice with MQ to remove any media. Following this, the wet weight of the EPS was recorded and then taken for lyophilization.



Fig 36: EPS 28 and EPS 35 after thawing post cryogelation. The yield for EPS 35 is visibly lesser.

Yield of EPS 28 vs EPS 35

The EPS isolation protocol was carried out under two temperature conditions, 28°C and 35°C. The washing steps revealed that 28°C consistently produced a higher yield of EPS compared to 35°C, suggesting the impact of temperature on EPS production and recovery. The wet weight of the EPS per 200 mL culture was recorded, averaging around ~5.6 g at 28°C and ~1.1g at 35°C, resulting in a yield ratio of 1.6:1 for 28°C to 35°C cultures.

	Grams (per 200 mL culture)	
	EPS 28	EPS 35
R1	5.63	1.22
R2	5.77	0.93
R3	5.53	1.31
Avg	5.64	1.15

Fig 37: Yield table recording the wet weight of Mp EPS at 28°C and 35°C.

Deproteinization of EPS

Prior to deproteinization, the lyophilized EPS was hydrated overnight in MQ. The deproteinization step utilized a carefully formulated buffer containing 100 mM Tris-HCl (pH 7.5), 4% SDS, 8 M urea, 2 M thiourea, and EDTA. After hydration, the pellet was incubated overnight at 70°C in 30 mL of this buffer to remove residual proteins. Post-incubation, the sample was washed extensively with MQ water. Each wash involved heating the sample to 95°C for 5 minutes, followed by centrifugation at 12,000 RPM for 10 minutes. This washing cycle was repeated 13-15 times until foam from detergent residues disappeared completely. Typically, no foam was observed after the 13th wash.

Reagent	Amount
100mM Tris-HCL (pH 7.5)	6.975 g
4% SDS	20 g
8M Urea	240.24 g
2M Thiourea	76.12 g
EDTA	1.213 g

Fig 38: EPS Deproteinization buffer (500 mL) with reagents listed in order of addition

Dialysis Process

Dialysis was initiated post-deproteinization to remove smaller molecules and residual impurities. The protocol began with preparing a 6 L jar of MQ water and washing a one kDa membrane thrice with MQ. The EPS sample was then loaded inside the

membrane, which was then sealed at both ends with clips. The membrane was placed vertically upright in the dialysis jar. Water was changed twice on the following day, once in the morning and once in the evening. After dialysis, samples were collected into 15 mL falcon tubes and stored at 4°C. The membranes were washed with MQ and stored in 1% sodium azide solution for reuse.

Appendix B – Publications/Conference Presentations

Presented a poster at the CARBO-XXXVIII: Recent Advances in Glycoscience and Glycotechnology, held in Guwahati, Assam, India, from December 4th to 6th, 2024.

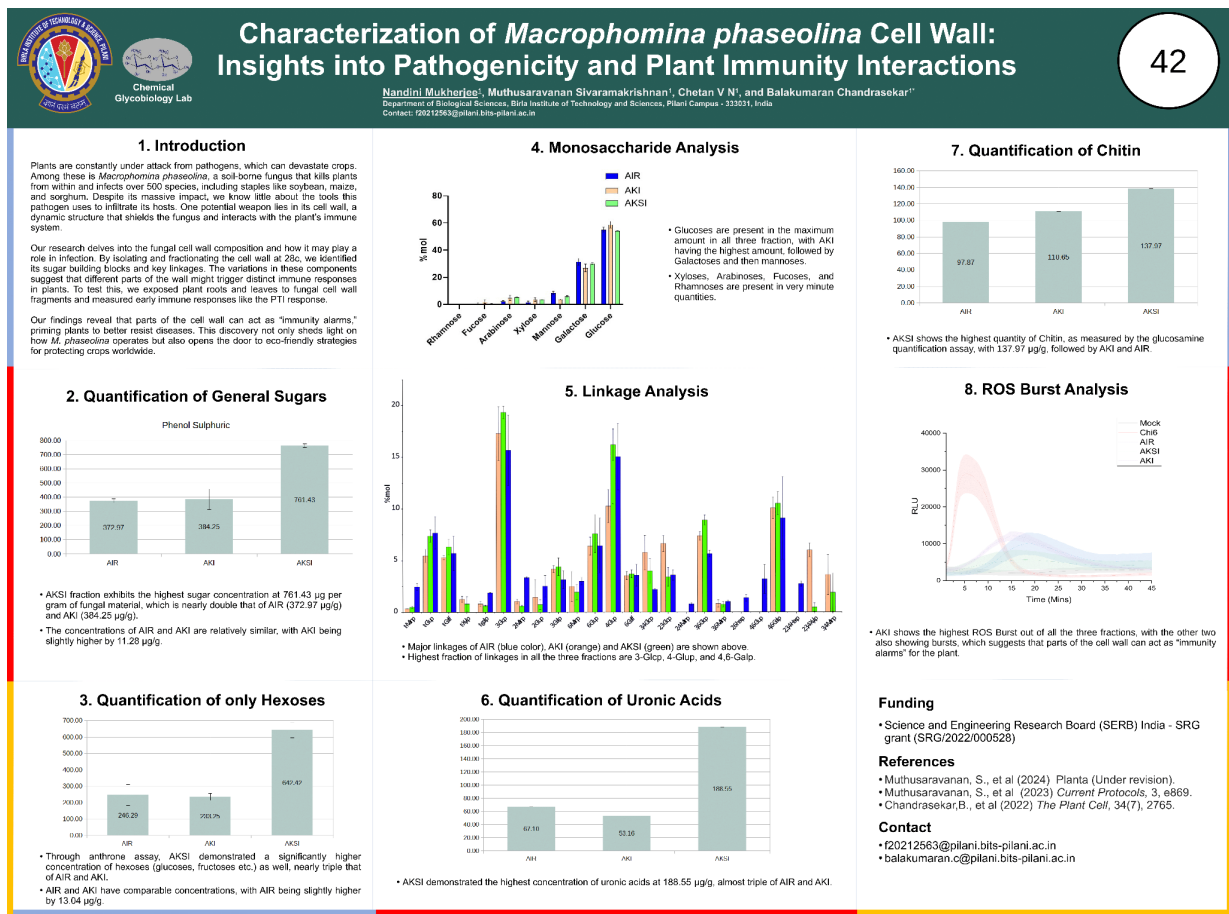


Fig 39: My poster for the CARBO-XXXVIII conference.